Interaction Between Antimicrobial Peptides and Non-lipid Components in the Bacterial Outer Envelope

by
© Sheyla Montero Vega

A thesis submitted to the
School of Graduate Studies
in partial fulfillment of the requirements for the degree of

Master of Science

Department of Biochemistry
Memorial University of Newfoundland

August, 2021

St. John's Newfoundland

Abstract

Antimicrobial peptides (AMPs) offer advantages over conventional antibiotics; for example, bacteria develop resistance to a lesser extent to AMPs than to small-molecule antibiotics. The interaction of the AMPs with the liposaccharide (LPS) layer of the gram-negative bacteria cell envelope is not well understood. I constructed a MARTINI model of a gram-negative bacterial outer membrane interacting with the AMP Magainin 2. In a 20 μs MD simulation, the AMP diffused to the LPS layer of the cell envelope and remained there, suggesting interactions between the Magainin 2 and the LPS layer causing the AMP to concentrate at that position. Furthermore, the free energy profile for the insertion of the Magainin 2 into the membrane was calculated using umbrella sampling, which showed that the AMP positioned such that the cationic sidechains of the AMP coordinated to the negatively charged phosphate groups of the LPS layer. These simulations indicate that AMPs partition into the LPS layer of a bacterial membrane.

Table of Contents

List of figures

List of tables

List of abbreviations

AMPs	Antimicrobial Peptides
LPS	Lipopolysaccharide
DNA	Deoxyribonucleic acid
RaLPS	Outer core of the Lipopolysaccharide
ReLPS	Inner core of the Lipopolysaccharide
Kdo	3-Deoxy-d-*manno*-oct-2-ulosonic acid
Hep	Heptose
Oant	O-antigen of the Lipopolysaccharide
MIC	Minimal inhibitory concentration
AMP:L	Molar AMP to lipid ratio
MD	Molecular Dynamics

GPU	Graphical processing units
POPE	1-Palmitoyl-2-oleoyl-sn-glycero-3-phosphoethanolamine
POPG	1-Palmitoyl-2-oleoyl-sn-glycero-3-phosphatidylglycerol
CDL2	Cardiolipin 2
WHAM	Weighted Histogram Analysis Method

Chapter 1: Introduction

1.1 Antibiotic resistance

Antibiotics are therapeutic molecules used for preventing or treating bacterial infections. The first documented use of antibiotics was by John Parkinson in the 19th century [1]. Alexander Fleming's discovery of penicillin started the revolution of antibiotics in the 20th century [1]. However, the easy access and overuse of antibiotics have led to bacterial resistance to antibiotics.

Antibiotic resistance is a natural phenomenon. Bacteria have large genetic plasticity that allows them to respond to environmental threats like antibiotics. To acquire resistance, bacteria have evolved mechanisms to avoid antimicrobial action. Mutations in the bacterial DNA or horizontal gene transfer can produce the acquired resistance [2]. The main mechanisms of resistance are as follows: the production of enzymes to degrade antibiotics [3] like the secretion of beta-lactamase into the periplasm [4]; the formation of efflux pumps that transport antibiotics out of the cell [5]; the modification of the target molecules of the antibiotics; and the modification of metabolic pathways used by the bacteria [2] (Fig.1).

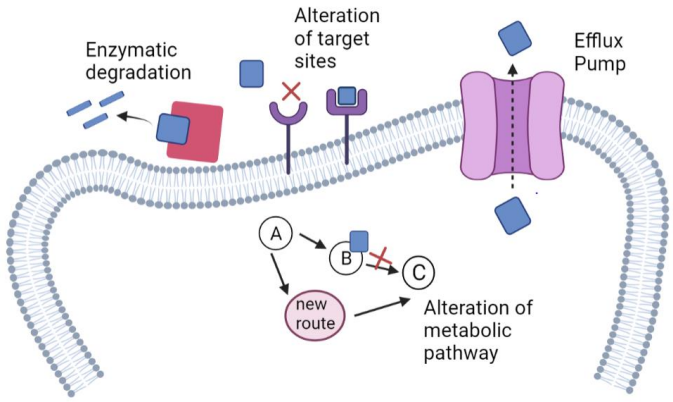

Fig.1.1: The mechanisms of resistance to antibiotics in bacteria include: Production of enzymes to degrade antibiotics, modification of the target molecules of the antibiotics, the production of efflux pumps that transport antibiotics out of the cell, and the modification of metabolic pathways used by the bacteria. (Created in biorender.com).

In the last decade, rates of antibiotic resistance to common bacteria like *Klebsiella pneumoniae* and *Escherichia coli* have escalated. Antibiotic resistance has led to a dangerous increase in multidrug resistance for pneumonia, tuberculosis, malaria, urinary tract infections, wounds, bloodstream infections, and others. Infections with antibiotic resistant bacteria increase the risk of bad clinical outcomes and death. The patients also consume more healthcare resources than patients infected with the same bacteria that do not demonstrate the same pattern of resistance [6].

The World Health Organization published a Global Report of Surveillance in 2014 stating that the number of infections caused by multidrug-resistant bacteria is increasing. Almost 2 million people in the United States are infected per year with resistant bacteria, causing 20 billion dollars of losses to the US economy. New antibacterial agents are needed for the treatment of bacterial infections. Antimicrobial peptides (AMPs) are a promising prospect for the basis of new antibiotic treatments [7].

1.2 Antimicrobial peptides

AMPs are effector molecules present in the innate immune system of a wide variety of organisms across all domains of life. The story of antimicrobial peptides goes back to 1939, when a substance isolated from *Bacillus brevis* call gramicidin, showed activity against a range of gram-positive bacteria. Gramicidin later became the first antimicrobial peptide to be commercialized for use as an antibiotic in topical treatments. The boom of antibiotics following the discovery of penicillin resulted in decreased interest in antimicrobial peptides. The lack of interest in AMP changed in the 1960s when multidrug resistant bacteria were discovered. The emergence of resistance to existing antibiotics spurred new research into AMPs. The first reported animal AMP was defensin, isolated from rabbit leukocytes in 1956 [8]. In 1963 it was proved that human leukocytes use AMP in their lysosomes [9]. Several groups in the 1970s and 1980s reported antimicrobial peptides produced from leukocytes, including α-defensins from rabbits and humans [10].

One important landmark in the history of antimicrobial peptides is the work of Boman *et al.* in 1981. Boman injected bacteria into pupae of a silk moth and isolated the antimicrobial peptides used by the pupae to defend against the bacteria [11]. These peptides were sequenced and

characterized, constituting the first α helical antimicrobial peptides reported. In another critical study Zasloff *et al.* isolated and characterized cationic antimicrobial peptides from the African clawed frog. These peptides were named Magainins [12]. To this day, more than 600 natural cationic antimicrobial peptides have been described, with examples from almost all domains of life [13].

AMPs can kill bacteria and fungi, and some are active against viruses and cancer cells [14]. AMPs offer a broad spectrum of antimicrobial activity. In addition to killing microorganisms, they also can induce an immune response. Antimicrobial peptides are diverse in the mechanism of action, structure, and sequence. A crucial advantage of AMPs is that they induce less resistance in bacteria [15]. Generally, AMPs do not interact with a specific protein receptor or enzyme. Instead, they act directly on the bacterial envelope by disrupting the membrane. While bacteria can develop resistance to protein-targeting antibiotics through the mechanisms described earlier, these mechanisms are less effective against membrane-disrupting AMPs [16].

1.3 Structure of antimicrobial peptides

AMPs are generally 12–50 amino acids in length, and even the largest AMPs are less than 150 amino acids in length. AMPs present in plants and animals are typically amphipathic and cationic, with excess arginine and lysine. The presence of positively charged amino acids suggests that these proteins could have attractive electrostatic interactions with the lipid headgroups of the outer membranes of bacteria, which are generally negatively charged. AMPs contain around 50% hydrophobic amino acids, which are essential to their interaction with the membrane. AMPs have various amino acid sequences that give a diverse secondary and tertiary structure [17]. There are four major classes of AMP according to their secondary structures: linear α-helical peptides, β-sheet containing peptides, extended linear structures, and peptides containing both α and β elements [18].

The α-helical peptides were one of the first AMP structure classes to be characterized [11]. This group of AMPs is the best studied; hundreds of natural peptides have been identified with this secondary structure. The synthesis of analogs has also contributed to the diversity of α-helical AMPs.

Most of these α-helical peptides are random coils in aqueous solutions. Their immersion in bacterial membranes stabilizes the α-helical conformations of the AMPs. As amphipathic peptides, AMPs can interact with the hydrophilic head and the hydrophobic tail of the membrane phospholipids [18]. The helical structures have a large variety of lengths and different content and orientation of charged and hydrophobic residues. This variety gives the range of activities of this class of peptides [17]. Amidation at the C-terminus, that is common in natural helical AMPs AMPs, increases the electrostatic interaction between the peptide and the negatively charged molecules in the bacterial membrane and enhances the activity of most helical AMPs.

1.4 Magainin

Magainins are a family of α helical AMPs discovered in the skin of the African frog *Xenopus laevis*. Magainins are promising candidates as a new type of therapeutic antibiotics because of their high efficacy in killing bacteria, while their toxicity against mammalian cells is low [19]. Magainin 2 is the most studied peptide in this family.

Magainin 2 has 23 amino-acids and a net charge of +4 at neutral pH (Fig. 1.2). Magainin 2 has an unfolded structure in solution, but it folds to an α-helical structure after contact with the membrane surface. The conformation inside the LPS layer is unknown (Fig. 1.2) [14]. Magainin 2 creates a local defect in the bacterial bilayer, forming disordered toroidal pores [20]. The toroidal pores permeabilize the bacterial membranes.

Magainin 2 can form dimers via a disulfide bond, and this dimerization is significant for their activity [21]. Homodimers of Magainin are more active than monomers [21].

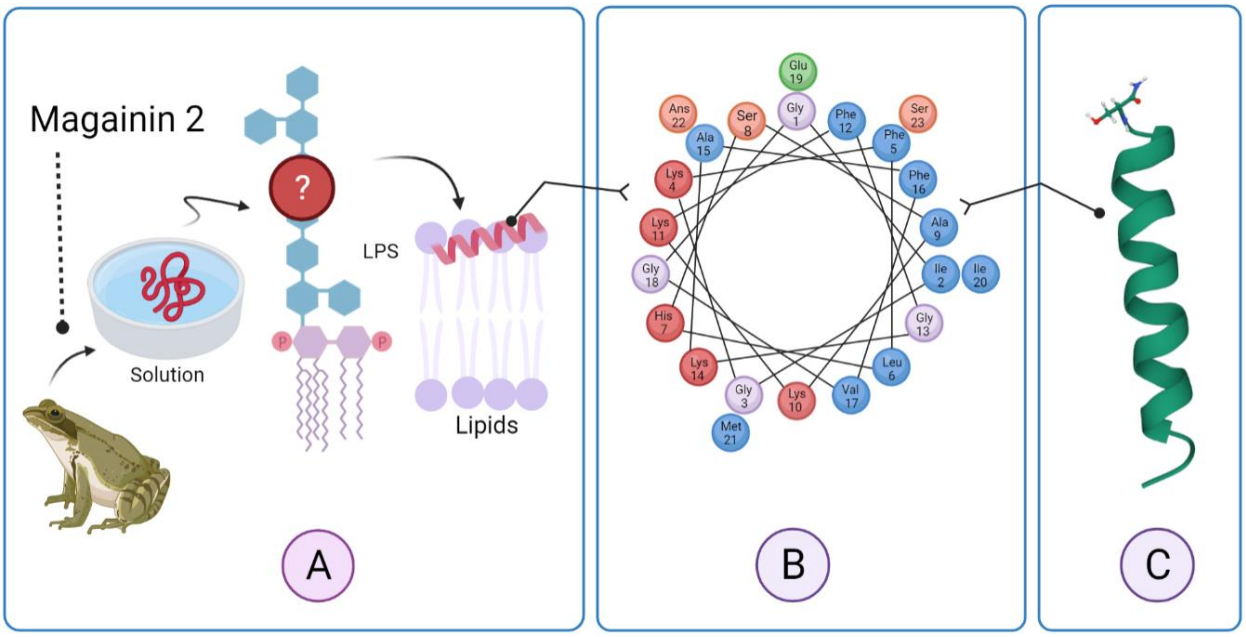

Fig. 1.2: A) Magainin 2 is extracted from Xenopus laevis. The structure is unfolded in solution, unknown in the LPS layer, and alpha helical in the membrane. B) The α helix of Magainin 2 is amphipathic. Blue: hydrophobic amino acids; red: positively charged amino acids; orange: polar amino acids; pink: Glycine; Green: negatively charged amino acids. C) Magainin 2 structure obtained by NMR in DPC micelles, downloaded from Protein Data Bank (PDB ID: 2MAG) [22], *(Structure in render in 3D VIEW of rcbc.org* [23]*). (Created in biorender.com)*

Magainin 2 has excellent activity and shows significantly lower cytotoxicity than many naturally occurring AMPs. However, Magainin 2 can lyse red blood cells, although its hemolytic activity is significantly weaker than other AMPs like melittin [24], and has poor biological stability toward proteolytic enzymes [25]. Magainin 2 has been used as a basis for creating synthetic analogs made by a series of amino acid substitutions, truncation of the peptide, and terminal modifications [26]. The purpose of these synthetic analogs is to make Magainin more active and improve its stability and safety.

Magainin 2 preferentially targets bacterial membranes over membranes of the cells of the host organism. Understanding how these peptides target the bacterial membrane is necessary for developing new peptides with more selectivity. Theories of how AMPs target specific bacteria focus on the difference between bacterial and eukaryotic cell envelopes. One of these differences is the composition; for example, the presence/absence of sterols, LPSs, peptidoglycans, and the charge of the polar head of the membrane lipid in the outer leaflet [14]. The cationic nature of

Magainin 2 could allow selective interaction with anionic components of the bacterial cell envelope, including lipids, as well as possibly the carbohydrate and other cell envelope components [27]. Eukaryotic membranes have a more significant proportion of lipids with neutral headgroups, so, in principle, their electrostatic interactions with the cationic groups of Magainin 2 would be weaker.

1.5 Bacterial Cell Envelope

The chemical composition of the cell envelope of bacteria is highly complex (Fig. 1.3). The cell envelope of gram-negative bacteria has an inner membrane, a peptidoglycan layer, and an outer membrane [28]. Between those layers is the periplasmic space, containing a variety of ions and proteins [29]. The outer membrane of gram-negative bacteria is a highly asymmetric bilayer. The outer leaflet is composed mainly of LPSs (LPS) (Fig. 1.3), while the inner leaflet of many gram-negative bacteria, including *Escherichia coli*, is composed of zwitterionic and negative phospholipids, mainly phosphatidylethanolamine and phosphatidylglycerol, as well as cardiolipins [7].

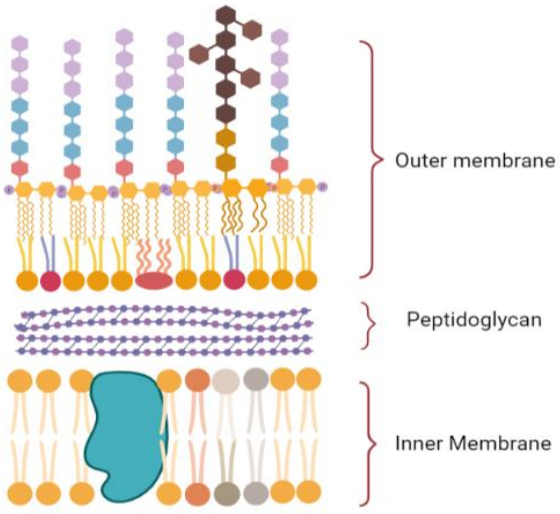

Fig. 1.3: The cell envelope of gram-negative bacteria is composed of: an outer membrane formed by a LPS layer and a phospholipid layer, a peptidoglycan layer and an inner membrane formed by a lipid bilayer (Created in biorender.com).

The LPS molecules (Fig. 1.4) are macromolecules composed of lipids and carbohydrate components covalently bonded with each other (Fig. 1.3). The LPS molecules have three main components. The first component is Lipid A, which acts as an anchor of the LPS to the membrane. Lipid A is the most conserved part of the LPS and consists of a disaccharide of D-glucosamine and two phosphate groups that are linked to positions 1 and 4. The disaccharide is substituted with six acyl chains linked by ester and amide bonds. The amino linked fatty acids are always (R)-3-hydroxy myristic acid, while the ester linked fatty acids can vary between myristate, laureate, or palmitate. The interaction between Lipid A negative charges and the divalent ion Mg^{2+} and Ca^{2+} is fundamental for the stability of the membrane.

The second component, linked to Lipid A, is a phosphorylated oligosaccharide chain known as the core. The core is divided into the outer core (RaLPS) proximal to O-antigen and the inner core (ReLPS) directly linked to Lipid A. The chemical structure of the inner core is conserved within each family of bacteria and usually contains residues of 3-deoxy-d-*manno*-oct-2-ulosonic acid (Kdo) and heptose (Hep) (Fig. 1.4). In contrast, the outer core has greater structural variability even inside different serotypes of the same bacteria. The composition of the core has an important role in the biological activity of LPS [30]. The core has an overall negative charge conferred by the phosphorylated groups.

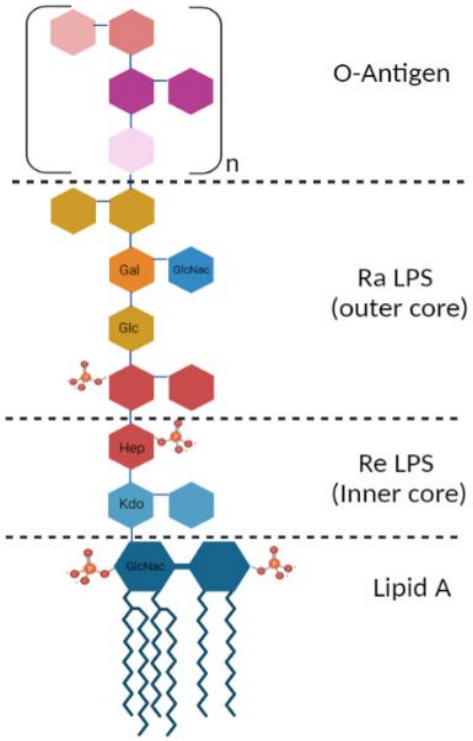

Fig. 1.4: LPS molecules are composed of: Lipid A formed by a disaccharide of D-glucosamine (blue, GlcNac) and two phosphate groups (red ball and stick models); the inner core formed by 3-deoxy-d-manno-oct-2-ulosonic acid (light blue, Kdo), heptose (red, Hep), and a phosphate group; the outer core formed by heptose (red, Hep), galactosamine (orange), glucose (brown), D-glucosamine (blue) and a phosphate group; and the last component the O-Antigen formed by repeated units made with 2–7 monosaccharides (pink, salmon, lilac) (created in Biorender.com).

The third component is a highly variable polysaccharide called O-antigen. The O-antigen has a variable number of repeated units made with 2–7 monosaccharides. The O-antigen can be branched or linear, and most are heteropolymers. The number of identified O-antigens is vast and constantly increasing. *Escherichia coli* alone produces more than 170 types of O-antigens [31]. The primary function of O-antigen in the bacteria envelope is thought to be protective; O-antigen may contribute to the evasion or delay of the immune responses in the host [32].

1.6 AMP mechanisms of action

The most widely accepted mechanism of action of AMPs is the direct targeting of the bacterial membrane, the disruption of the lipid bilayer, and the permeabilization process [29]. The cationic and hydrophobic composition of most AMPs makes them suitable for interacting with and

disturbing bacterial membranes that are mainly anionic. After the initial contact of the AMPs with the lipids through electrostatic interactions, the peptide permeabilizes microbial membranes and dissipates the electrochemical gradient across the membrane. The permeabilization of the membrane results in the disruption of the cell function, including vesiculation, fragmentation, the release of DNA, cell aggregation, and destruction of cell morphology [33].

The discussion about mechanisms is mostly centered on how the AMPs destabilize and permeabilize the membrane. The carpet mechanisms and the toroidal pore are the most widely accepted models (Fig. 1.5) [34]. The classical model for toroidal pores is a well-ordered structure with lipids and peptides intercalated, forming a transmembrane channel. The ordered toroidal pore assumes that the pore is cylindrical, and the peptide is parallel or perpendicular to the pore [19]. Recently, the disordered toroidal pore has been proposed as an alternative to this traditional model [20]. In this model, the inside of the pore is not well organized and has an irregular arrangement. In the disordered toroidal pore, the peptides do not line on the pore and can bind to the membrane surface after pore formation. The disordered toroidal pore was described and observed in simulations for melittins [20] and Magainin [35] and is believed to be a general mechanism for the formation of pore in AMPs.

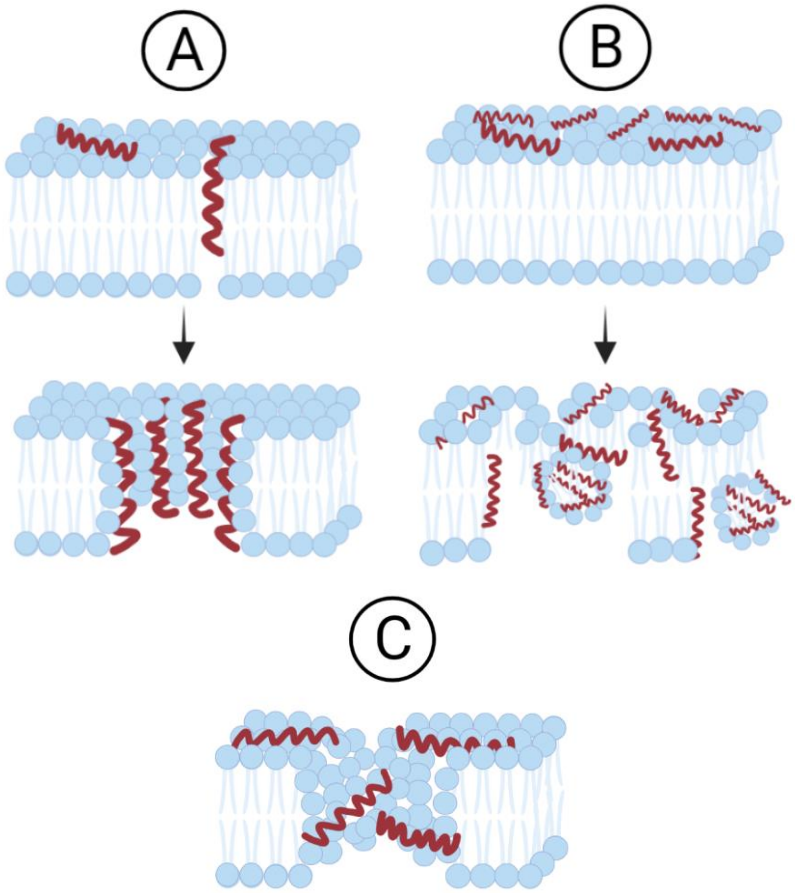

Fig. 1.5: A) The toroidal model. AMPs insert into the membrane and induce the lipid layer to bend continuously through the pore. B): The carpet model. The AMPs disrupt the membrane by forming micelles. At a critical concentration, the AMPs form transient holes in the membrane. C) The disordered toroidal pore. The pore is not well organized and has an irregular arrangement. (created in biorender.com).

The carpet model is a non-pore forming model where the AMP acts through a mechanism similar to detergents. In this model, a high density of peptides interacts parallel to the membrane surface. The high ratios of peptide/lipid in the membrane produce the displacement of phospholipids, leading to the disruption of the membrane [33]. Other models exist for the interaction of AMPs and membranes, like the detergent model and barrel-stave model [7].

How AMPs initially interact with bacterial cell envelopes and ultimately affect them is still poorly understood. Most of the studies about the mechanism of action and the permeabilization of AMPs are carried out in synthetic liposomes [36]. Unifying and connecting the result from *in vitro*

experiments and experiments with the whole bacteria is challenging. In experiments where the AMP is exposed to whole bacterial cells, the minimal inhibitory concentration (MIC) is a parameter used to compare the efficiency of antibiotics. The MIC is the lowest concentration required for AMPs to limit the growth of the bacteria.

The molar AMP to lipid ratio establishes a direct comparison between *in vitro* experiments in liposomes and experiments in the whole bacteria. Wimley calculated that the minimum dose of AMP needed for membrane permeabilization is 10000 times higher in bacteria than in liposomes [36]. This result suggests that an AMP interacting with bacteria binds to other molecules that are not present in liposomes. Multiple researchers have suggested that the LPS layer of the bacterial membrane is the component that AMPs are interacting with [37][38]. Significantly, experiments on *E. coli* mutants where the LPS layer was absent had a lower MIC, indicating that the presence of the LPS layer makes AMPs less effective [37]. The possible interactions between the AMPs and the LPS on the cell wall of gram-negative bacteria can change our views on the mechanism of action AMPs.

In 1994, Hancock [39] proposed that the uptake of AMPs occurs through a mechanism similar to the mechanism established for traditional antibiotics. According to this "self-promoted uptake" hypothesis, the cationic AMPs initially interact with the negative charge of the LPS layer in the outer membrane. This first interaction displaces the Mg^{2+} or Ca^{2+} ions that stabilize the LPS layer by neutralizing the charges. Under this hypothesis, the peptide-LPS interaction distorts the acyl chains in the outer layer, then inserts into and translocate across the bilayer (Fig. 1.6) [39].

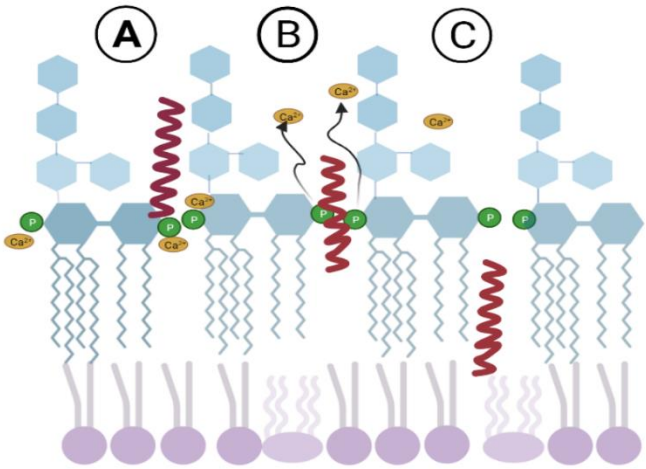

Fig. 1.6: The "self-promoted uptake" of AMPs. A) AMP first interacts with the LPS layer. B) The peptide displaces ions that crosslink Lipid A, destabilizing the LPS layer. C) Insertion of the AMP in the membrane (created in biorender.com)

Even though the self-promoted uptake hypothesis was proposed 25 years ago, the details about the interactions between the LPS layer and cationic peptides that would provide evidence in support or opposition to this hypothesis are still non-existent.

Another hypothesis about the function of the bacterial envelope's components proposed that the LPS layer can act by trapping the AMP [40]. The LPS can act like an electrostatic barrier capturing AMPs and preventing the insertion in the lipid hydrophobic core. These questions about the function of the LPS layer have not been answered. More data about the affinity of the AMPs for the cell wall components are needed [41].

Understanding how AMPs interact with the bacterial outer membrane and the LPS layer would aid the development of synthetic peptides that retain the membrane-disrupting features of natural AMPs while also improving features important for practical use, like selectivity of the bacterial cell over host cells.

Computer simulations are one approach for elucidating the interactions between AMPs and a biological membrane. Molecular dynamics (MD) methods have become essential techniques for the study of complex membranes. MD simulations of AMPs interacting with model bacterial membranes could help resolve which mechanism for AMP interaction is correct.

1.7 Molecular Dynamics Simulations

MD is a powerful technique that can simulate the motion of a large number of particles using Newton's laws of motion. These simulations yield a trajectory that shows the dynamics of the particles throughout a simulated time. These trajectories can be analyzed to calculate time-averaged equilibrium distributions that show the equilibrium structure of the system, the probabilities of occupying the available conformational states, and the physical properties of the system. In this thesis I discuss a subset of the classical MD simulation that have been widely used to study biomolecules like proteins, lipids, nucleic acids, glycan, and more complex structures like biomembranes. For these systems, molecular dynamic simulations act like a "computational microscope"[42], allowing us to describe a system at an atomistic resolution level, sometimes with more detail than standard biophysical experiments can provide. Improvements in computing hardware (e.g., Graphical Processing Units, GPUs) and simulation algorithms have made it possible to simulate larger systems, for longer time intervals, with greater accuracy.

1.7.1 Force Field

Molecular dynamic simulations require that both the intramolecular and intermolecular forces of the system are calculated accurately at every step of the simulation [43]. These calculations are made using a "force field", which is a mathematical expression and a set of parameters used for determining the potential energy of a chemical system given the positions of the particles in the system. The total potential energy in a force field includes bonded and non-bonded interactions (Fig.1.7) (Eq 1.1).

$$\upsilon_{total} = \upsilon_{bonded} + \upsilon_{non-bonded} \qquad \text{Eq (1.1)}$$

The bonded interactions (Eq 1.2) are between atoms that are connected with covalent bonds. The most basic mathematical form of the bonded potential energy includes three terms, . The first term uses Hooke's law to describe bond stretching. The second term again uses Hooke's law to describe angle bending. The third term describes rotation about a torsion or dihedral angle (Eq

1.2). Other terms can be as well included like dihedral cross-terms, quartic angle terms, and other forms of improper angles.

$$v_{bonded} = \sum_{bonds} \frac{1}{2} k_{bond} (r - r_e)^2 + \sum_{angles} \frac{1}{2} k_{angle} (\theta - \theta_e)^2 + \sum_{dihedrals} k_{\phi} (1 + \cos(n\phi - \delta)) \quad \text{Eq (1.2)}$$

where k_{bond} and k_{angle} are force constants, r_e is the equilibrium length, θ_e is the equilibrium bond angle, k_{ϕ} is the barrier height, n is the periodicity of the term, ϕ is the torsional angle, and δ is the offset.

The non-bonded equation (Eq 1.3) describes the interactions between any pair of atoms that are not connected and are within a given cut-off radius. These terms include the van der Waals interactions, described by a 6-12 Lennard-Jones potential, and the electrostatic interaction between partial charges, described by a Coulombic potential (Eq 1.3). Other bonded interaction terms can included 12-10 potentials, explicit multipole terms, Buckingham potentials, and others.

$$v_{non-bonded} = \sum_{pair:ij} 4\varepsilon_{ij} \left[\left(\frac{\sigma_{ij}}{r_{ij}} \right)^{12} - \left(\frac{\sigma_{ij}}{r_{ij}} \right)^{6} \right] + \frac{q_i q_j}{4\pi\varepsilon_0} \frac{1}{r_{ij}} \quad \text{Eq (1.3)}$$

where ε_{ij} is the van der Waals well depth, σ_{ij} is the atomic radius, r is the distance between the particles in question, q is the partial atomic charge, ε_0 is the permittivity of the free space.

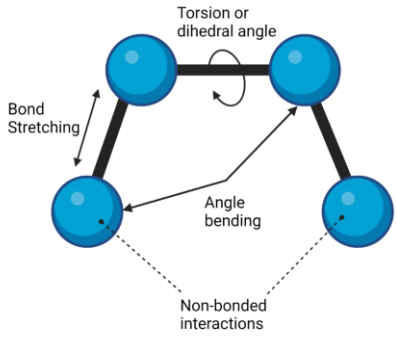

Fig 1.7: The total potential energy in a force field includes bonded and non-bonded interaction. The bonded interactions are: the bond streching, the torsion or dihedral angle and the angle bending. The non-bonded interactions include the van der Waals interactions, described by a 6-12 Lennard-Jones potential, and the electrostatic interaction between partial charges. (Created with biorender.com)

A set of these parameters must be defined for a force field to be used in a simulation. The accuracy of a molecular dynamic simulation is directly dependent on the quality of the force field parameterization. There are several force fields available for simulations of biomolecular lipid and protein containing systems, e.g. CHARMM [44], [45], AMBER [46], [47], Slipids [48], GROMOS [49].

1.7.2 Coarse-Grained Models

In many popular molecular mechanical models, each atom is represented as an explicit particle; this gives us a very structurally precise model describing all the atoms. These simulations are costly in terms of computational resources and require a long time to produce results, especially for simulations of bio-membranes. Biological membranes are complex biochemical structures formed from a variety of lipids, carbohydrates, and membrane proteins. For these types of membranes, equilibration times increase to microseconds, and equivalently long simulations are needed to investigate any aspect of the system. Because of the large size of these systems, the computational cost of these simulations is prohibitive, even with modern computing hardware [41].

Consequently, to save resources and time, we should consider interactions relevant to the problem in question and cut down the number of atoms in the system. This goal was the basis for

the development of the coarse-grained method of simulations. The use of coarse grain models or all-atom models depends on what we are trying to study in our systems and the simulation time required for seeing the process. For studies of structural details in proteins or changes in the structures all-atom models are adequate. In contrast for long membrane processes like AMP insertion in the membrane, coarse-grain models enable the necessary simulation time to be reached.

The parameterization of the force field depends on the model's level of resolution. The full atomistic details of force fields have higher resolution and are usually parameterized using properties obtained from the experimental calculation of quantum mechanics. With the need to perform simulations of systems with a higher spatiotemporal range, lower resolution levels of force fields like coarse-grained have been developed [50].

In coarse-grained models, atoms are grouped into functional groups, reducing the number of particles in the system. This kind of model groups 3–6 heavy atoms (i.e. C, O, N) and their associated hydrogens in a coarse-grained bead particle. The use of bead particles immediately reduces the number of interacting particles by a factor of 3–6. An indirect benefit of this coarse-graining is that these models tend to have a smoother energy landscape, leading to faster dynamics and the ability to use larger time steps [51]. The computational power needed to perform the simulations is reduced, and both the size and simulation time of the system can be simultaneously increased.

The use of coarse-grained models for lipids started in the 90s with the work of Smit in water-oil interfaces. A large diversity of coarse-grained approaches is available, ranging from qualitative models to models with a high level of chemical specificity. Some models treat the solvent implicitly and do not have bead particles that explicitly represent solvent molecules [52], while others explicitly represent the solvent [53].

The parametrization of coarse-grained force fields includes two approaches: the top-down or structure-based and the bottom-up or thermodynamically-based. In the bottom-up approach, the data for constructing the models is obtained directly from all atom simulations or structure databases. The top-down models reproduce experimental data-like thermodynamic properties.

Many coarse-grained models use a combination of both strategies to minimize the limitations derived from using either approach alone [42].

1.7.3 MARTINI models

MARTINI is a coarse-grained force field used in the simulation of a broad range of biological systems, developed by the laboratories of Marrink and Tieleman [51]. MARTINI combines top-down and bottom-up parametrization strategies. Even though this force field was generated from atomistic models, it does not entirely focus on reproducing the structural details at a particular point. MARTINI models have a limited chemical and spatial resolution compared with all-atom simulations but allow for longer simulations of larger systems. The development the MARTINI force field involved an extensive calibration of non-bonded interactions against thermodynamic data [54].

The MARTINI force field makes the simulation of membranes and a wide range of membrane related processes possible. This model is based on modular building blocks. Typically, 4 heavy atoms and their associated hydrogens are mapped in a single bead. This modularity makes possible the parametrization of many biomolecules including glycolipids, cardiolipins, polysaccharides, sterols, proteins, carbohydrates, and nucleotides [51].

The mapping of atomistic structures to a MARTINI model takes roughly 4 non-hydrogen atoms (and the hydrogens atoms bonded to them) and maps them into a single MARTINI bead. This ratio was selected to make the model computationally efficient while still capturing the type of chemical distinctions present in biological molecules. In some instances, a higher level of resolution is needed for a chemical motif. For example, the ring structures present in some amino acids are mapped with more resolution by including only 2 non-hydrogen atoms in each bead. For water, 4 molecules of water are mapped in one bead. Ions are represented in one bead that represents the ion and its first hydration sphere [51].

In the MARTINI model, beads are assigned one of four main types: polar (P), non-polar (N), apolar (C), and charged (Q). Within each type, they can be distinguished by a letter according to their capabilities for hydrogen bonding: donor (d), acceptor (a), both (da), and none (0). They also

have a number indicating the degree of polarity from low polarity (1) to high polarity (5). Based on this classification, in the version of the MARTINI force field used in this thesis, 18 different types of beads have been defined [54] (Table 1.1).

Table 1.1: Well depth in Lennard-Jones potential in kJ/mol for non-bonded interactions between the 18 different types of beads (adapted from Reference [54]*) .*

TYPE OF BEAD		Q				P					N				C				
		da	d	a	0	5	4	3	2	1	da	d	a	0	5	4	3	2	1
Q	da	5.6	5.6	5.6	4.5	5.6	5.6	5.6	5.0	5.0	5.0	5.0	5.0	3.5	3.1	2.7	2.3	2.0	2.0
	d	5.6	5.0	5.6	4.5	5.6	5.6	5.6	5.0	5.0	5.0	4.0	5.0	3.5	3.1	2.7	2.3	2.0	2.0
	a	5.6	5.6	5.0	4.5	5.6	5.6	5.6	5.0	5.0	5.0	5.0	4.0	3.5	3.1	2.7	2.3	2.0	2.0
	0	4.5	4.5	4.5	3.5	5.0	5.6	5.0	4.5	4.0	4.0	4.0	4.0	3.5	3.1	2.7	2.3	2.0	2.0
P	5	5.6	5.6	5.6	5.0	5.6	5.6	5.6	5.6	5.6	5.0	5.0	5.0	3.5	3.1	2.7	2.7	2.3	2.0
	4	5.6	5.6	5.6	5.6	5.6	5.0	5.0	4.5	4.5	4.0	4.0	4.0	3.5	3.1	2.7	2.7	2.3	2.0
	3	5.6	5.6	5.6	5.0	5.6	5.0	5.0	4.5	4.5	4.5	4.5	4.5	3.5	3.5	3.1	3.1	2.7	2.3
	2	5.0	5.0	5.0	4.5	5.6	4.5	4.5	4.5	4.5	4.5	4.5	4.5	4.0	3.5	3.5	3.1	2.7	2.3
	1	5.0	5.0	5.0	4.0	5.6	4.5	4.5	4.5	4.5	4.5	4.5	4.5	4.0	3.5	3.5	3.5	3.1	2.7
N	da	5.0	5.0	5.0	4.0	5.0	4.0	4.5	4.5	4.5	4.5	4.5	4.5	3.5	3.5	3.1	2.7	2.7	2.7
	d	5.0	4.0	5.0	4.0	5.0	4.0	4.5	4.5	4.5	4.5	4.0	4.5	3.5	3.5	3.1	2.7	2.7	2.7
	a	5.0	5.0	4.0	4.0	5.0	4.0	4.5	4.5	4.5	4.5	4.5	4.0	3.5	3.5	3.1	2.7	2.7	2.7
	0	3.5	3.5	3.5	3.5	3.5	3.5	3.5	4.0	4.0	3.5	3.5	3.5	3.5	3.5	3.5	3.5	3.1	2.7
C	5	3.1	3.1	3.1	3.1	3.1	3.1	3.5	3.5	3.5	3.5	3.5	3.5	3.5	3.5	3.5	3.5	3.1	3.1
	4	2.7	2.7	2.7	2.7	2.7	2.7	3.1	3.5	3.5	3.1	3.1	3.1	3.5	3.5	3.5	3.5	3.1	3.1
	3	2.3	2.3	2.3	2.3	2.7	2.7	3.1	3.1	3.5	2.7	2.7	2.7	3.5	3.5	3.5	3.5	3.5	3.5
	2	2.0	2.0	2.0	2.0	2.3	2.3	2.7	2.7	3.1	2.7	2.7	2.7	3.1	3.1	3.1	3.5	3.5	3.5
	1	2.0	2.0	2.0	2.0	2.0	2.0	2.3	2.3	2.7	2.7	2.7	2.7	2.7	3.1	3.1	3.5	3.5	3.5

Non-bonded interactions between beads consist of Lennard-Jones interactions and coulombic interactions as described by equation 1.3. The strength of the Lennard-Jones interaction depends on the value of the well-depth (ε) of two interacting beads. There are 10 levels of the interaction strength between the 18 types of beads (Table 1.1). The value of ε ranges from 2.0 kJ/ mol for the interaction between polar and apolar beads to 5.6 kJ/ mol for interaction between the polar beads. This difference in interaction strength gives rise to the hydrophobic separation of the polar and apolar components of the system [54].

One fundamental parameter for MARTINI models is the cut-off radii for the non-bonded potentials. The non-bonded interactions are cut off at a distance of 1.2 nm; both the energy and the force vanish at this distance. The Lennard-Jones potential is shifted from r_{shift} = 0.9 nm to r_{cut} = 1.2 nm. The use of this shifting potential mimics the effect of a distance-dependent screening and decreases the interaction strength to zero in a continuous manner. This switching function also

ensures the interaction potential is continuous, which is a requirement for stable MD simulations. The non-bonded interactions are parameterized using thermodynamic data like free energy of hydration, the free energy of vaporization, and partitioning free energy between water and organic phases (ether, octanol, chloroform, hexadecane)[51].

The bonded interactions are described by a standard function of bonds, angles, and dihedrals (Eq 1.2). The Lennard-Jones interactions are excluded between bonded particles. The MARTINI model describes the stretching of the bonds between beads using a weak harmonic potential (ν_{bond}) (Eq 1.4). The chain stiffness is described by adding weak harmonic potentials for the angles formed between sets of three beads (ν_{angle}) (Eq 1.5). The proper dihedral in the MARTINI model imposes a secondary structure, while improper dihedrals prevent out-of-plane distortions of planar groups. The parametrization of bonded interactions uses structural data from atomistic simulations and atomistic geometries obtained from experiments (e.g., X-ray crystallographic structures from the Protein Data Bank) [51].

$$\nu_{bond}(R) = \frac{1}{2} k_{bond}(R - R_{bond})^2 \qquad \text{Eq (1.4)}$$

$$\nu_{angle}(\theta) = \frac{1}{2} k_{angle}[\cos(\theta) - \cos(\theta_0)]^2 \qquad \text{Eq (1.5)}$$

Were, k_{bond} and k_{angle} are force constants, R_{bond} is the equilibrium length, θ_0 is the equilibrium bond angle.

The grouping of multiple atoms into more massive beads and the softer potential energy terms makes it possible to use larger timesteps in MARTINI MD simulations compared to the time steps employed in atomistic simulations. Most systems can be simulated with the MARTINI model with an integration time step of 20–40 fs compared to the 2 fs time step typically used in all-atom models. The smaller number of particles, the simplified potential energy expression, and the larger timestep make the MARTINI model hundreds or thousands of times more efficient than the equivalent all-atom simulations [42].

One notable limitation of the MARTINI models is the absence of an explicit treatment for hydrogen bonding interactions. As a result, these models are not suitable for simulations of protein folding or conformation isomerization. They cannot describe the dynamic formation of hydrogen bonds between units of the amide backbone, which is fundamental for the proteins' secondary and tertiary structure. In practice, in most instances where a MARTINI model is being used to model a protein-containing system, the protein is force by additional restraining forces to remains in its native , folded state throughout the simulations; no changes occur in its secondary structure. Elastic models have been applied to restrain the protein close to its initial structure in instances where the protein could isomerize to a non-physical state if only the MARTINI model was used [42].

1.7.4 Simulation of the Outer Bacterial Membranes

Due to the chemical complexity of the bacterial membrane, specifically, the presence of the LPS layer, modeling the outer membrane of gram-negative bacteria is still challenging. The coarse-grained model and force field for three types of LPS have only been developed recently [55]. There are only a few simulation studies with bacterial envelopes and AMPs that include the LPS layer and practically none include the O-antigen level [56]–[58].

The first atomistic model for a bacterial envelope containing the LPS layer was reported in 2012 by Kirschner *et al.*[59]. This model only contains the ReLPS part of the LPS molecule. In the past year, new models have been developed, including coarse-grained models.

A all atom simulation of the whole cell envelope with a realistic membrane composition was reported in 2018 to study of the distribution of mechanical stress [60]. The outer layer of this membrane included an entire LPS layer, two types of phospholipids, membrane proteins, and ionic species [60]. In another study, the influence of Polymyxin B1, one of the most potent AMPs, in the LPS layer was explored in 2017 by Hsu *et al.*[58]. The model construct was a coarse-grained MARTINI bilayer of only LPS molecules without O-antigen, in the presence of two different ions. They showed the effect of the peptide in inducing the formation of crystalline patches in the membrane [58].

The use of only one type of phospholipid or LPS for mimicking the entire cell envelope was used in most of the early membrane simulations for simplicity and more efficient sampling. The use of model membranes with multiple components and more realistic lipid mixtures is increasingly become more common. The importance of using a mixture of phospholipids closer to the accurate bacterial membrane composition has become increasingly apparent. The utilization of more complex cell envelopes, including realistic LPS molecules, for studying the mechanism of AMPs is a necessity [61]. The development of CHARMM-GUI was a major step forward in making this type of simulation practical. The CHARMM-GUI website service offers a fully automatic solution for building lipid bilayers with various sizes, lipid compositions, and asymmetry. The CHARMM-GUI includes all-atom LPS models from various bacterial species and coarse-grained models for the three types of LPS present in *E. coli*. In the last year, a coarse-grain model for O-antigen was made available [56].

1.8 Simulation Methods

1.8.1 Periodic Boundary Conditions

Periodic boundary conditions (Fig. 1.8) are used to allow a smaller system to mimic a macroscopic system. A relatively small simulation cell is replicated infinitely, with particles interacting with particles inside the simulation cell as well as their periodic images. When a particle moves from the primary simulation cell into a periodic image, it simultaneously re-enters the simulation cell from the opposing face of the simulation cell. This allows the properties of a much larger system to be estimated based on the properties of a small simulation cell and avoid the need to include unrealistic interfaces at the boundary of the system. The size of the system needs to be carefully considered since even a small system can lead to artefacts and deviation from experiments.

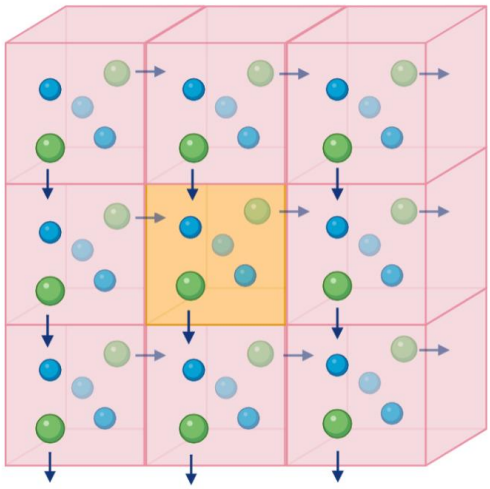

Fig.1.8: Periodic boundary conditions. A simulation cell (yellow) is replicated infinitely. As a particle moves from the primary simulation cell into a periodic image, it simultaneously re-enters the simulation cell from the opposing face of the simulation cell. (Created in biorender.com).

1.8.2 Thermostats and Barostats

The isothermal-isobaric ensemble is a thermodynamic ensemble where the number of particles, the pressure, and the temperature, are constants, but energy can transfer between the system and the surroundings. The thermostat and barostat control the temperature and the pressure of the system. The three most common thermostats are Nosé–Hoover, Berendsen, and stochastic velocity thermostats.

The Berendsen thermostat is an algorithm that scales the velocity of the particles in the simulation to control the temperature. When this thermostat is applied, the system is weakly coupled to a heat bath that holds the target temperature for the simulation, but it does not sample a rigorous statistical ensemble [62]. The stochastic velocity rescaling thermostat is based on the Berendsen thermostat but has an extra stochastic term that scales the velocities using kinetic energy from the Maxwell–Boltzmann distribution [63]. The Nosé–Hoover thermostat adds an extra term to the equations of motion to transfer energy to and from the system. Although these thermostats introduce artificial forces that slow or speed the particles in the system, if the thermostat is chosen

judiciously, it will sample the target thermodynamic ensemble efficiently without causing the dynamics of the simulation to be unrealistic [64].

Barostats scale the dimension of the simulation box for controlling the pressure. Two of the most popular barostats are the Parinello–Raham and the Berendsen (that act similarly to the equivalent thermostat) and the Nosé–Hoover. The Parinello–Raham barostat is an extension of the Nosé–Hoover barostat that allows pressure coupling to be applied separately to each dimension of the simulation cell. This barostat also allows cell stress to be regulated, as well as pressure. These barostats also add additional terms to the equations of motion.

1.8.3 Umbrella Sampling Simulations

MD simulations sample a Boltzmann distribution of states, so the lowest energy regions of configurational space are sampled exponentially more than higher-energy states. Theoretically, suppose an unbiased simulation is given enough time. In that case, the simulation will sample the entire energy surface, but the presence of energy barriers and the significant range of energies makes it practically impossible to sample the entire energy surface within a feasible timescale. As a result, the energy barriers prevent crossing from one low-energy state to another low energy state, even after several μs. Even with the increase of computational power in the last decade and the use of coarse-grained models to study biological systems, correctly sampling the higher energy (but nevertheless important) states of the complex biological model is still an issue.

For AMP–membrane interactions, the AMP's membrane position can be defined in terms of the difference of the AMP center of mass and the center of mass of the membrane along the Z coordinate. In an unbiased MD simulation, the AMP only occupies some of the positions on this coordinate, making it impossible to quantitatively identify the most stable location of the AMP within the membrane or the energetics of the insertion.

Enhanced sampling techniques are one solution to accelerating sampling of the configurational space, other possible solutions are building faster computers. Umbrella sampling is one of the most popular techniques for enhanced sampling [65]. To perform an umbrella sampling simulation, a series of "windows" are simulated. These windows are the same except

that a different artificial force is applied that restrains a molecule along the Z coordinate. Each window is biased to sample a specific part of the configuration space. The AMP position is restrained with a harmonic bias:

$$v_{bias}(s) = \frac{1}{2}k(s - s_0)^2 \qquad \text{Eq (1.6)}$$

Where k is the spring constant and s_0 is the reference position of the restraint. The distribution sampled by this simulation will be:

$$P'(q) \propto \mathrm{P}(q)e^{-v_{bias}(s)/k_BT} \qquad \text{Eq (1.7)}$$

where $\mathrm{P}(q)$ is the unbiased distribution.

Combining the simulation with different values of S_0, we can obtain a continuous set of simulations and sample all positions along the coordinate. For large values of k, only points close to S_0 will be sampled. For simulations of AMP-membrane interactions, umbrella sampling can be used to sample the full range depths to which the AMP is inserted into the membrane and to sample a complete free energy profile.

1.8.4 Potential of the mean force

After performing the biased simulations, I need to find the unbiased probability distribution given the umbrella sampling histograms and compute the potential of the mean force (a.k.a, the free energy profile along coordinate Z). This distribution can be obtained by performing Weighted Histogram Analysis Method (WHAM). The WHAM equations are [66]:

$$P(Z) = \frac{\sum_{i=1}^{N_w} {g_i}^{-1}\, h_i(Z)}{\sum_{j=1}^{N_w} n_j\, {g_j}^{-1} \exp\left[-\beta\left(w_j(Z) - f_j\right)\right]} \qquad \text{Eq (1.8)}$$

and

$$\exp(-\beta f_j) = \int dz \exp\left[-\beta w(z)\right] P(Z) \qquad \text{Eq (1.9)}$$

where P(Z) denotes the unbiased probability, β is the inverse temperature ($\frac{1}{k_b T}$), f_j is the free energy constants, k_B is the Boltzmann's constant, T is the temperature, n_j is the total number of data points in histogram h_j. The statistical inefficiency g_i is calculated with the integrated autocorrelation time τ_i of umbrella window i, $g_i = 1 + 2\tau$.

The P(Z) is related to the free energy profile via Eq 1.10:

$$\mathcal{W}(Z) = -\beta^{-1} \ln\left(\frac{P(Z)}{P(Z_0)}\right) \qquad \text{Eq (1.10)}$$

where z_0 is an arbitrary reference where $\mathcal{W}(Z_0)$ is 0. The WHAM equations must be solved iteratively to obtain the unbiased distribution. The convergence of the WHAM equations depends on the number of histograms and the overlap of adjacent windows on the free energy profile.

Hypothesis

The first interaction between AMPs and the bacterial cell envelope is still poorly understood. There are two main hypotheses of how the AMPs interact with the LPS layer in gram-negative bacteria. One of these hypotheses is the self-promoted uptake of the AMP that proposes the necessity of first interaction with the LPS layer. In the self-promoted uptake mechanism, the cationic AMPs initially interact with the LPS layer's negative charge in the outer membrane. This first interaction displaces the Mg^{2+} or Ca^{2+} ions that stabilize the LPS layer. Under this hypothesis, the peptide-LPS interaction distorts the acyl chains in the outer layer, then inserts into and translocate across the bilayer. Another hypothesis about the function of the bacterial envelope's components

proposes that the LPS layer can act by trapping the AMP. The LPS can act like an electrostatic barrier capturing AMPs and preventing the insertion in the lipid hydrophobic core. Even with the growing interest in AMP action in the whole bacteria with the LPS layer, neither of these two ideas have evidence to back them up. Computational studies can help and elucidate and characterize the interaction between AMPs and non-lipid components of the bacterial outer membrane using MD. The working hypothesis for my work is that the antimicrobial peptide Magainin 2 has a first interaction with LPS layer in the bacterial cell envelope.

Chapter 2: Methods

2.1 Simulation Details

All simulations were performed using GROMACS 2018.1 nano (MD parameters in Appendix 6.1) [67] with the standard simulation options for the MARTINI model. The dynamics were propagated using the leap-frog integration algorithm (integrator = md). A 0.02 ps time step was used. The center of mass velocity of the membrane was removed every step using the linear mode.

The simulations were performed using periodic boundary conditions. The system was simulated in the isothermal-isobaric ensemble with a bath temperature of 310 K and an external pressure of 1.0 bar using the stochastic velocity rescaling thermostat and Parinello-Rahman barostat. The non-bonded Lennard-Jones and Coulombic interactions were smoothly reduced to zero at 1.2 nm using a switching function in our simulations. A neighbor list was constructed for each atom and is updated every 10 steps.

2.2 Membrane Construction and Composition

I constructed a coarse grain model for a bacterial membrane with the MARTINI 22 force field, including the MARTINI 2.2 amino acids, MARTINI 2.0 lipids, and non-polarizable water. I constructed the model using the CHARMM-GUI web interface [68], specifically the MARTINI bilayer maker [28], [58], [69].

The model of the inner layer was composed of a realistic mix of phospholipids in *E. coli* (Table 2.1). The system contained 90% of the total number of membrane molecules of 1-Palmitoyl-2-oleoyl-sn-glycero-3-phosphoethanolamine (POPE), 5% of 1-Palmitoyl-2-oleoyl-sn-glycero-3-phosphatidylglycerol (POPG) and 5% cardiolipin 2 (CDL2). The inner layer composition had 640 lipids where 576 are POPE, 31 are POPG and 32 are CDL2 [70]. The outer layer was composed fully of 218 molecules of Lipid A and a mix of 50% of the core oligosaccharide (RaLPS) and 50% of O-antigen (OANT) (Table 2.1) [58].

The membrane was solvated with 36740 coarse-grained non-polarizable water molecules, 534 Na^+ cations, 1090 Ca^{2+} dications, and 441 Cl^- anions. The concentrations of Na^+ and Cl^- were adjusted to achieve neutrality in the simulation cell.

Table 2.1. Composition of the outer membrane simulation cell.

Outer layer composition		**Inner layer composition**		**Ions**	
RaLPS	109	POPE	576	Na^+	534
OANT	109	POPG	32	Cl^-	441
		CDL2	32	Ca^{2+}	1090

One molecule of the AMP Magainin 2 was added in the simulation cell to simulate the AMP–bilayer interactions. I downloaded the structure of Magainin 2 (PDB ID: 2MAG, model number 1) from the Protein Data Bank from the RCSB organization [23]. These structures were determined using two dimensional H-NMR spectroscopy of Magainin 2 in dodecylphosphorylcholine (DPC) micelles [22]. The PDB of Magainin 2 corresponds to an α-helical structure with 23 amino acids. A series of modifications to the PDB file were necessary.

Using the pdb2gmx from Gromacs 2016, the c-terminal residue serine 23 was amidated with a neutral C-terminal group (i.e., a charge of 0). Histidine 7 was set to its neutral state (i.e., charge of 0) because at pH 7 Magainin 2 has been reported to have a total charge of +4 and the histidine residue not charged [22]. The model Magainin 2 used in our simulations had a total charge of +4, consistent with the experimental net charge at pH 7 [22].

The protein/membrane system was constructed using the MARTINI bilayer maker from the CHARMM-GUI website [68]. The AMP was positioned at +6 nm from the center of the membrane.

2.3 Equilibration

The simulation of a coarse-grained asymmetrical outer bacterial membrane, with LPS in one leaflet and phospholipid in the inner leaf, requires long simulation times to reach complete equilibration. The long simulation times are partly because the LPS layer is stiffer than a phospholipid layer [71]. Fig. 2.1 shows the change in the potential energy of the simulation cell throughout the MD. The potential energy of the system decreases systematically over the first 15 μs of the simulation. The equilibration results from of the membrane model spontaneously rearranging to form more energetically - favorable interactions between the components. After the 15 μs mark, the potential energy plateaus and fluctuates around the average -1.79×10^6 kJ/mol for the remaining 10 μs, indicating that the system has reached an equilibrium. Posterior analysis of the membrane and the study of interaction with the AMPs were performed using this equilibrated membrane structure (i.e., after 25 μs).

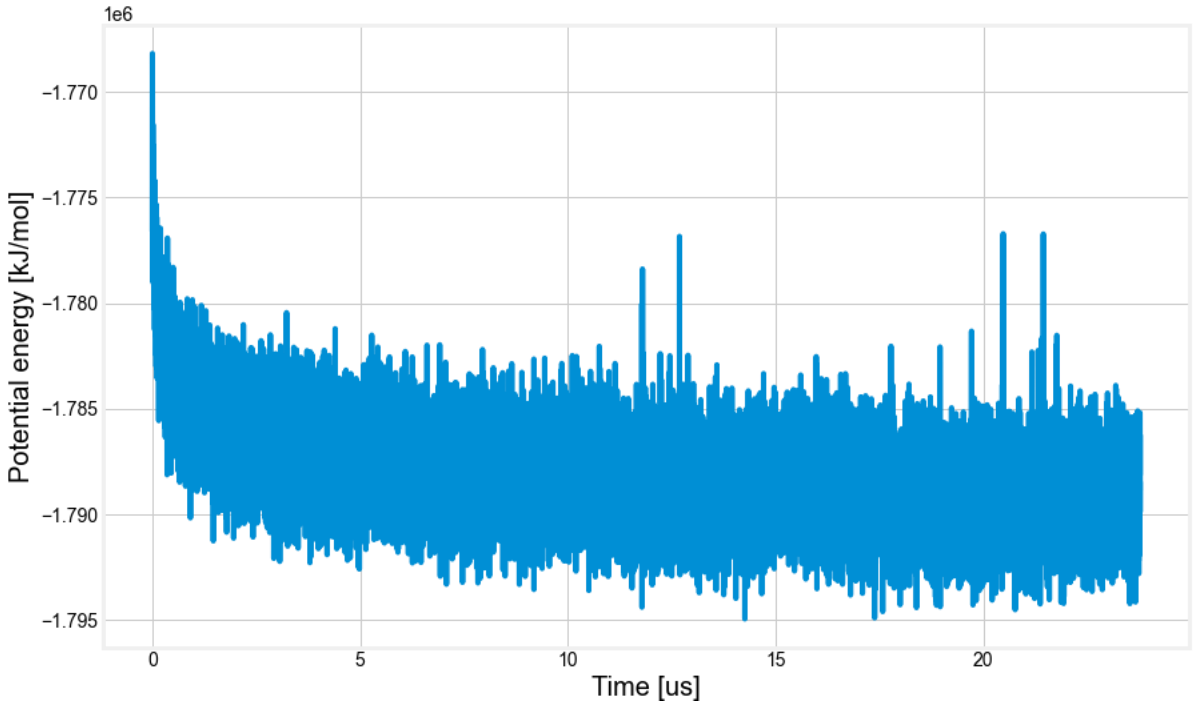

Fig.2.1: Equilibration of potential energy for the bacterial outer membrane model. After 15 µs *the membrane reached the equilibrium and fluctuated around the average -1.79 × 10^6 kJ/mol for the remaining 10 µs.*

2.4 Umbrella Sampling Simulations

Although several interesting results came out of the unbiased simulation, in order to get a complete view of AMP-outer membrane interactions for AMP positions within the membrane that were not observed in the unbiased simulations I need enhanced sampling techniques. For this I employed an umbrella sample approach, which is challenging because of the size and the complexity of the composition of the membrane (i.e. presence of RALPS and O-ANT) and the size of the AMP. To achieve convergence and a realistic free energy profile hundreds of simulations where needed, and different spring constants where tried in order to guarantee the sampling of each position of the membrane and guarantee overlap between windows (a.k.a the AMP positions in each simulation frustrated around a value, for a correct sampling the AMP positions in each simulation should partially overlap with the AMP positions in the next simulation).

In my research I performed umbrella sampling simulation for 216 peptide positions with the Magainin 2 peptide restrained every 0.1 nm from -10.7 nm to +10.9 nm. The initial coordinates for each window of the umbrella sampling simulations were obtained from a steered MD simulation, beginning from the structure where the AMP was in solution above the membrane.

In steered MD, a time dependent external force is applied to the system. I use the MOVINGRESTRAINT bias from the software PLUMED v2.6 [72], and add a time-dependent harmonic restraint to a structural variable of the system (eq 2.1).

$$V(\vec{s}\,, t) = \frac{1}{2}k(t)(\vec{s} - \vec{s}_0(t))^2 \qquad \text{eq (2.1)}$$

where k is the spring constant and $\vec{s}$ is the position. Both terms are time (t) dependent.

In our simulation, steered MD was used to pull the Magainin 2 peptide center of mass across the Z coordinate of the simulation box with a spring constant of 5000 kJ/mol advancing 0.1 nm every 1000 simulation steps (Input file for plumed steered MD in Appendix 6.2) (Fig. 2.2). I obtained 216 windows from the steered MD simulation. These 216 windows were the starting points for the umbrella sampling simulation.

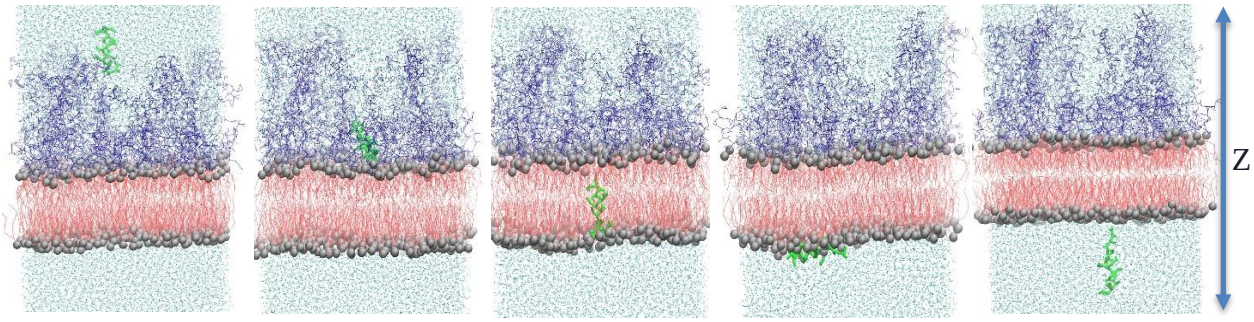

Fig. 2.2: Screenshots of 5 different time steps of the steered MD. The Magainin peptide (green) is pulled with a spring force of 5000 kJ/mol along the Z direction of the simulation box.

I performed 1 μs of umbrella sampling simulations in a total of 216 windows with the GROMACS-PLUMED/2019.5 software. The harmonic bias was applied with a spring constant of 1500 kJ/mol for the 216 simulation windows from -10.7 nm to +10.9 nm (input file in appendix

6.3). With the goal of improving the sampling, extra simulations were performed. I ran 101 simulation windows with a spring constant of 4500 kJ/mol and 18 simulations windows and with a string constant of 9000 kJ/mol.

2.5 Free energy profile

To calculate the free energy profile, I used the code WHAM version 2.0.11 from the Grossfield lab [73]. For the calculation of the free energy profile, the input file was constructed with:

1. the 336 output files from the umbrella sampling simulations with the position of the peptide in the simulation time and the bias-free energy,
2. the position restraint of the peptide
3. the values of the spring constant for each window.

The calculation of the free energy profile of Manganin 2 insertion into the bilayer required extensive simulations, and because of the slow rate of diffusion of the LPS layer and the size of the AMP it hard to achieve converged simulations. In trying to achieve convergence I performed 336 simulations which gave the combination of windows where all the AMP positions where were well sampled. The temperature of the umbrella sampling simulations was 323 K. Although this temperature is higher than the physiological temperature, it is generally necessary to compute the free energy profile of biological membranes with the LPS layer at elevated temperatures to achieve convergence [74]. Other factor than contribute to the convergence is using just the data of the equilibrate simulation, for this I discarded the data for the first half of the simulation was discarded.

Chapter 3: Results and Discussion

3.1 Analysis of the Bacterial Cell Envelope Structure

The first task was to assess the characteristics of the novel bacterial envelope structure I'd constructed. The composition of the membrane varies as a function of depth, which the density profile can quantify. The depth is typically measured relative to the membrane center of mass, and the Z coordinate is defined along the normal to the membrane plane. The density is calculated as a function of depth by analyzing the trajectory from a long MD simulation. The probability of finding a given component of the system at a particular Z position is calculated for each step and then averaged. I calculated the density profile in the last 1 μs of simulation using Gromacs command gmx_density. The density profile agrees well, in the positions of all the peaks, the water profile, and hydrophobic thickness, with the one reported for previous computational studies in LPS−DPPE membranes [75], [76]; this demonstrated that the model is robust at simulating critical elements of the bacterial membrane [77].

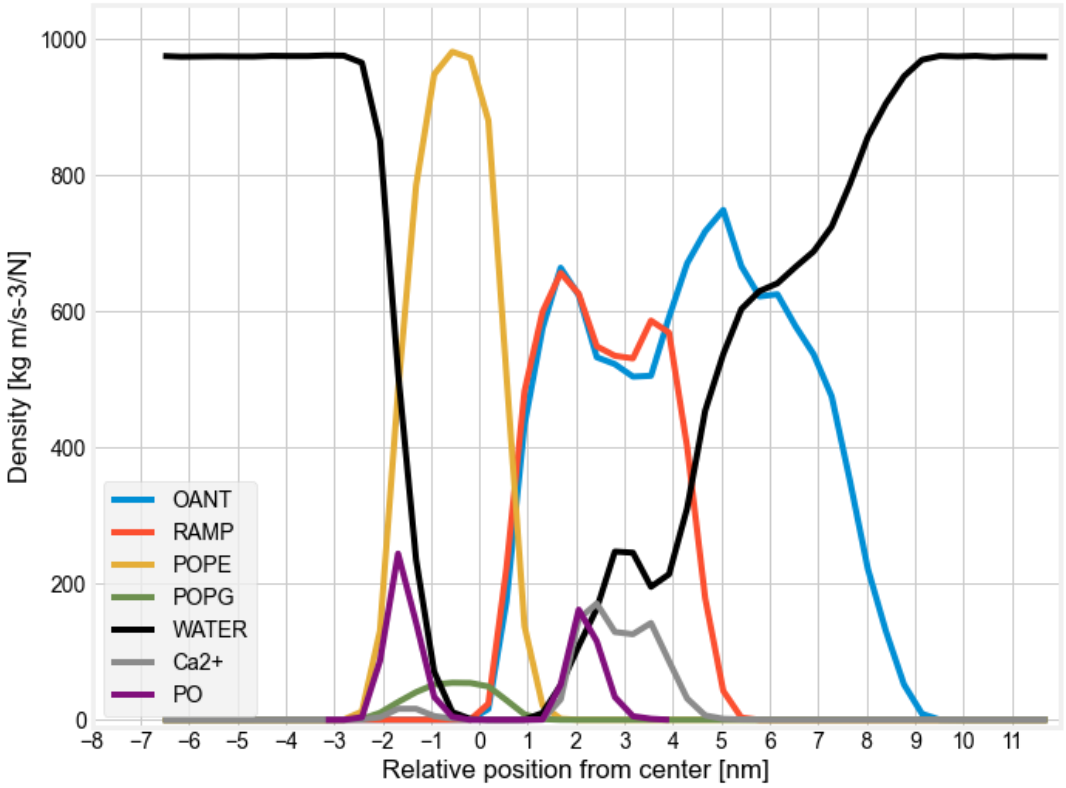

Fig. 3.1: The partial density analysis of membrane components along the Z coordinate.

I calculated the density profile for the OANT, RAMP, POPC, POPE, Ca^{2+}, water, and phosphate groups in the Lipid A and inner layer. The density profile for the phosphate groups has a peak of 200 kg/m^3 at -2 nm and +2 nm from the center of the membrane. The POPE has a peak from –2.5 nm to +1.5 nm. The maximum of the peak is at +1.5 nm with a density of 1000 kg/m^3. The POPG groups have a density peak from –2.5 nm to +1.5 nm, with a small maximum at +1.5 nm of 5 kg/m^3. The RAMP density peak goes from 0 nm to +5.5 nm with two maxima, one at +1.5 nm with a density of 660 kg/m^3 and the second at +3.5 nm with 600 kg/m^3. The OANT density profile has a density peak from 0 nm to +9 nm, with two maxima, one at 1.5 nm with a density of 660 kg/m^3 and the second at +5 nm of 750 kg/m^3. The Ca^{2+} peak goes from +1.5 nm to +5 nm with two maxima at +2 nm and +3.5 nm with a density of 150 kg/m^3.

The water density profile shows bulk water concentration (998 kg/m^3) in the interval of -7 nm to -3 nm. The water concentration drops sharply in the phosphate region of the lipid layer (-3 nm

to -1 nm) and reaches zero at the center of the POPE tails (i.e., the relative position of 0 nm). This is consistent with conventional phospholipid bilayers, where the headgroups are hydrated, but the water is almost completely absent from the hydrophobic lipid tail region. The LPS leaflet shows a more complex hydration structure. The density of water declines to 200 kg/m^3 between +9 nm and +4 nm, before having a minor second peak at the 3 nm point where the RAMP concentration is high. The density of water drops to zero at 1 nm, giving a hydrophobic thickness of the membrane of +2 nm (-1 nm, +1 nm). In previous computational studies of the outer bacterial membrane, the values of hydrophobic thickness are from +1.6 nm to +2 nm [78]. The water profile in our work is consistent with the reported atomistic water profile and previous coarse grain water profiles for the bacterial outer membrane [75].

The POPE/POPG peaks are concentrated in the –2.5 nm to +1.5 nm range. This density profile agrees with the density profiles of coarse-grained outer membranes formed by a mixture of POPE and POPG in the inner layer [76]. The range of the peaks for POPE and POPG shows a small difference at +0.4 nm with the range of these peaks in atomistic membrane profiles. For POPE, the maximum is the interior of the hydrophobic core, around the +1.5 nm point. The density at thisz depth is 1000 kg/m^3. Previously reported coarse grain and atomistic membranes with POPE alone in the inner layer reported a maximum at the same position in the interior of the hydrophobic core with a density of 1200 kg/m^3, so our simulations are in general agreement with theirs [76] [79].

The RAMP density profile starts at the center of the membrane (0 nm) and has a first peak at 1.5 nm. This maximum corresponds to the hydrophobic tail of the Lipid A in the RAMP. The location of this peak is in perfect agreement with the peaks for the computational model reported by Hughes *et al.* [76] for the terminal methyl group and methylene chains in Lipid A. The phosphate peak at 2.0 nm is part of the Lipid A molecule head groups. This peak is in the same position reported for the Lipid A head group [76]. The second maximum in the density profile of RAMP is at 3.5 nm. This peak represents the inner core carbohydrates, i.e. the RAMP molecules. The last section of RAMP ends at 5.5 nm and corresponds to the outer carbohydrate core. The second maximum and the last section correspond with the profile reported for RAMP by Hughes *et al.* [76].

The OANT density profile has the same behavior as that for the RAMP for the section from 0 to +2. This section corresponds to the Lipid A density profiles that is the same structure for both types of LPSs. The second and third peak of the OANT corresponds with the carbohydrate chain of the O antigen part of the OANT LPS.

The Ca^{2+} peak (Fig. 3.1) shows a small maximum around -2 nm; this peak is not present in atomistic models. The discrepancy in the presence of the peak in -2 nm between coarse-grained and atomistic models' density profiles was previously reported [79]. This peak is a product of a portion of the Ca^{2+} ions in the cell moving to the other side of the simulation box in long simulations due to the boundary conditions. It is not seen in atomistic simulation because the simulation times are usually not long enough for the counter ions to move through the boundaries. The second Ca^{2+} peak is at the same position of the Lipid A phosphate groups peak, and the third peak is in the LPS core phosphate groups region. This is consistent with the function of Ca^{2+} in the bacterial outer membrane. Based on the localization of Ca^{2+} ions in this region, I can conclude that the primary role of Ca^{2+} in these model membranes is to serve as counterions that stabilize and enable crosslinking contacts between the phosphate groups of the LPS layers.

3.2 Analysis of the unbiased MD simulation of Magainin 2 in the bacterial outer membrane

In the unbiased simulation with the peptide and the outer membrane, I did not observe an insertion of the AMP Magainin 2 in the membrane. After a few microseconds of simulation, I can see from a visual inspection that the peptide moves to the LPS layer of the bacterial outer membrane. After 20 μs of simulation, the AMP position in the Z direction maintains a relatively constant position in the LPS layer (Fig. 3.2).

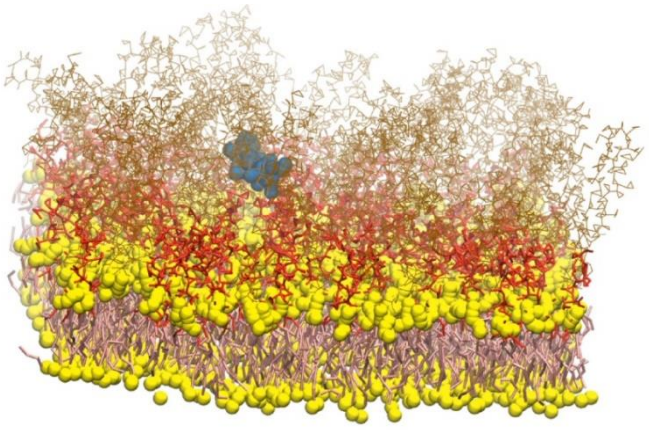

*Fig. 3.2: Bacterial outer membrane simulation snapshot at the 20 µs. The AMP, Magainin 2 is in th**e** LPS layer during the entire simulation time*

The calculation of the distance between the AMP center of mass and the membrane center in the Z coordinate shows a decrease after the first microsecond of simulation (Fig. 3.3). From 5 µs to 20 µs, the average distance of the AMP maintains a relatively constant value of between 5 nm and 5.3 nm from the center of the membrane.

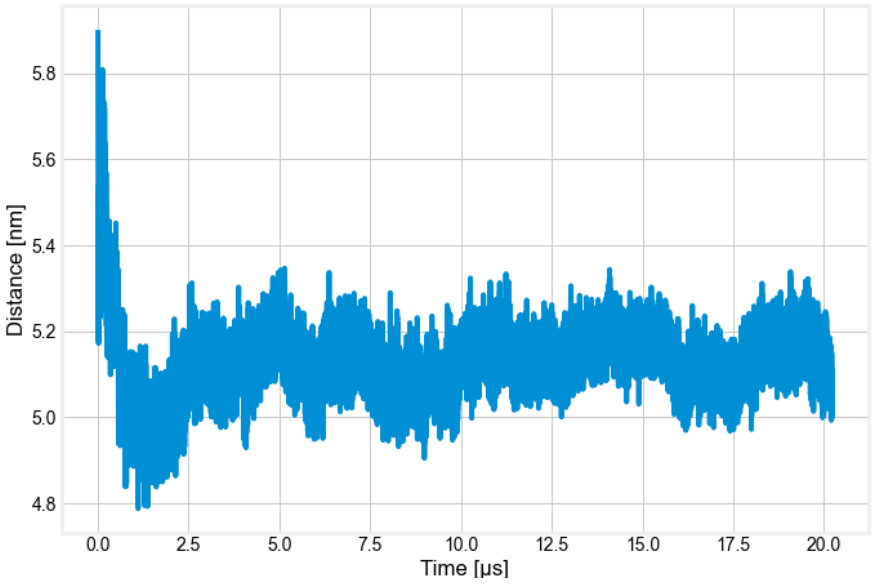

Fig.3.3: Distance from the membrane's center to the AMP's center of mass in the Z coordinate vs. time. The AMP was at ~ 5.1 nm for most of the simulation time.

The inspection of the unbiased simulation using the software VMD v1.9.3 for the trajectory (Fig. 3.2) and the calculation of the distance from membrane center to the peptide center of mass (Fig. 3.3) show that in the free simulation, the AMP stays in the LPS layer. The position of the AMP suggests a possible interaction between the AMP and the negative charges of the LPS layer.

Two main hypotheses can explain the position of the AMP in the cell envelope during the simulation based on the peptide's interaction with the LPS. One hypothesis is the "self-promoted uptake" of the AMP (Fig. 1.6). In this hypothesis, the positively charged amino acids of the AMP interact with the phosphate groups of the LPS layer. In the second hypothesis, the presence of an electrostatic barrier makes the AMP stay in the LPS layer in the unbiased simulation.

Further analysis is necessary to discriminate between these hypotheses. For the size of the simulation and the system complexity I need to perform techniques like umbrella sampling to sample the entire energy surface and determine the free energy of insertion of the AMP in the bacterial envelope. As well, more detailed analysis between the LPS phosphate groups and the AMP is needed. I first analyze the interaction of AMP and LPS phosphates groups by calculating the contact number and the minimal distance between both groups.

The contact number is the number of atom pairs that fall within 0.6 nm; it computes the number of contacts between two groups within that minimum distance. In my research, I calculated the contact number for each amino acid in the AMP Magainin 2 and the phosphate groups in the LPS layer. After this, I average the contact numbers for each amino acid and obtain the contact number for the full AMP sidechain (Fig. 3.4).

I can see an increase of the average LPS/AMP contact number over the 25 μs simulation time from 0.1 to 0.5. This increase to 0.5 is the reported average contact number for membranes with an LPS layer crosslinked with Ca^{2+}. In contrast, membranes linked with monovalent ions reported higher values of contact numbers [71]. The LPS molecules linked with divalent ions have less frequent interaction with the LPS layer than those crosslinked with monovalent ions. Hsu *et al.* [68] said that the LPS layer that is crosslinked with Ca^{2+} ions have a more rigid packing and can more effectively shield the phosphate groups from the AMPs than LPS crosslinked with Na^{+} ions.

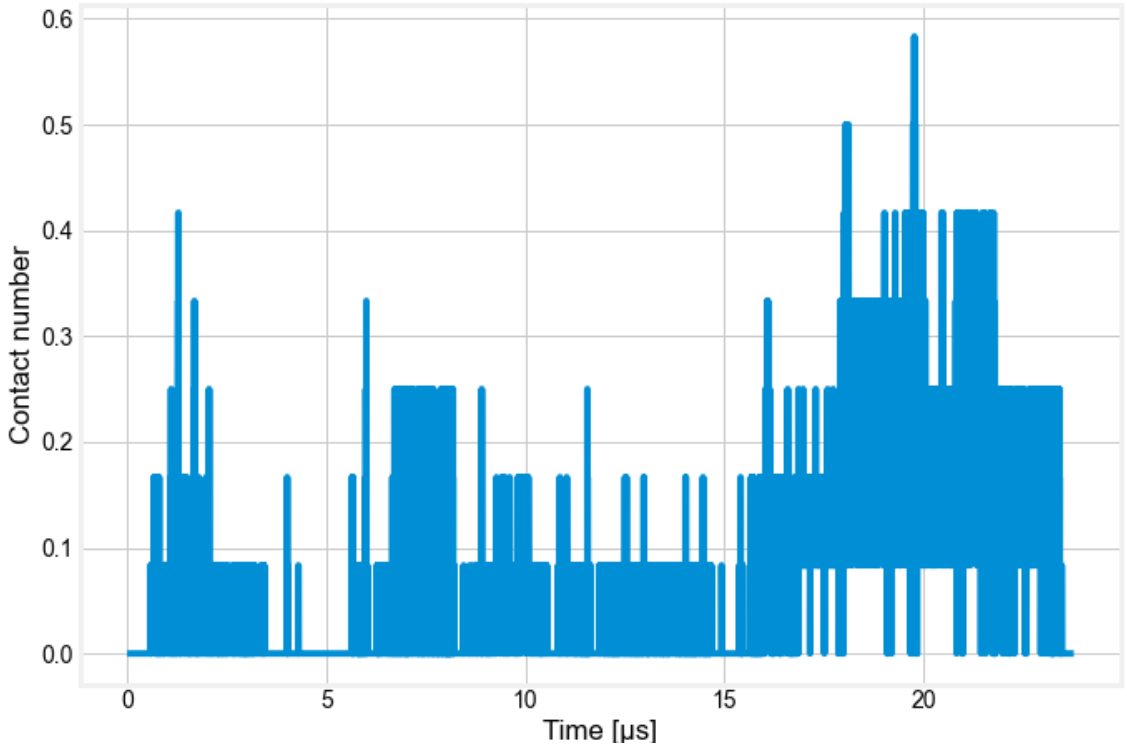

Fig.3.4: Average contact number between phosphates groups in LPS and sidechain of AMP for 25 μs MD simulation.

When the AMP is located deeper in the membrane, the interaction between phosphates in the LPS layer and the AMP can be obtained by calculating the minimum distance between the phosphate groups and the AMP (Fig. 3.5). The minimum distance was calculated for every amino acid sidechain and averaged to obtain the total AMP sidechain distance to the phosphate groups. For the entire 25 μs of the simulation, the AMP oscillates around 1.2 nm from the phosphate groups without getting closer than 1.0 nm. This is likely a limitation of unbiased MD simulations; even after 25 μs, the AMP could not displace the Ca^{2+} ions from their position next to the anionic phosphate groups. In the last μs of simulation the distance increase to +1.6 nm , this can be a product of fluctuation in position during the simulation.

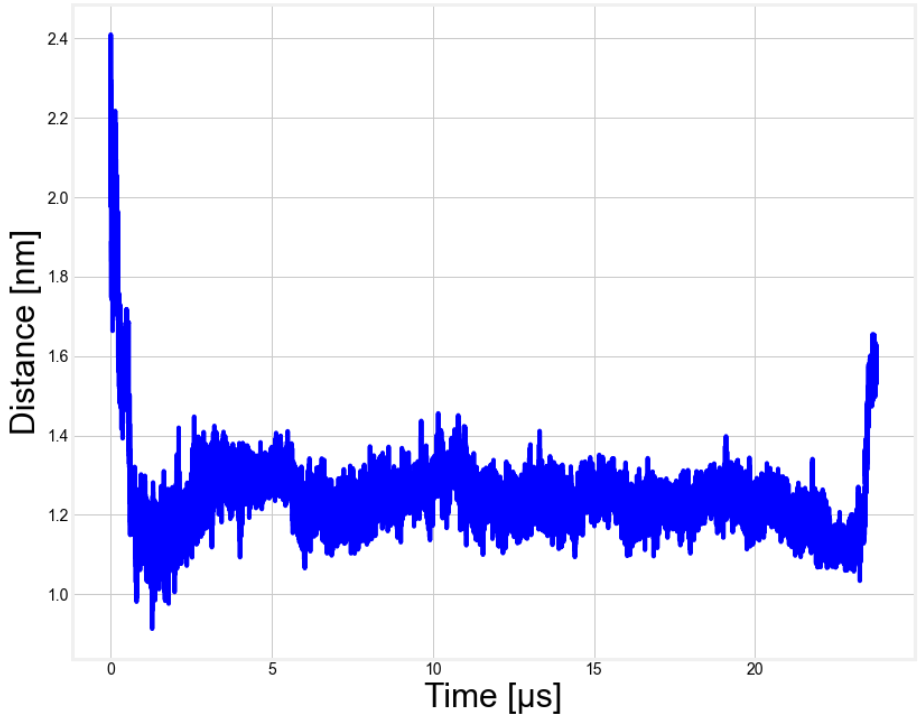

Fig. 3.5. Average distance between phosphates groups in LPS and sidechain of AMP for 25 μs. The average distance is 1.2 nm in almost all the simulation time.

Comparing membranes crosslinked with Ca^{2+} to those without Ca^{2+} can help us understand the interaction of the AMP with the lipopolysaccharide, specifically the function of Ca^{2+} in the interaction of the AMP with the LPS phosphate groups. I model two identical membranes crosslinked with Ca^{2+} and without Ca^{2+} and compare the average distance between the AMP sidechain and the LPS phosphate groups in both membranes (Fig. 3.6). The average distance from AMP to the phosphate groups in the simulation without Ca^{2+} ions is 0.85 nm, in contrast with the 1.2 nm in the simulation with Ca^{2+} ions. This shorter distance in the absence of calcium could be a product of an increase in interactions between the positively charged amino acids in the AMP and the phosphate groups.

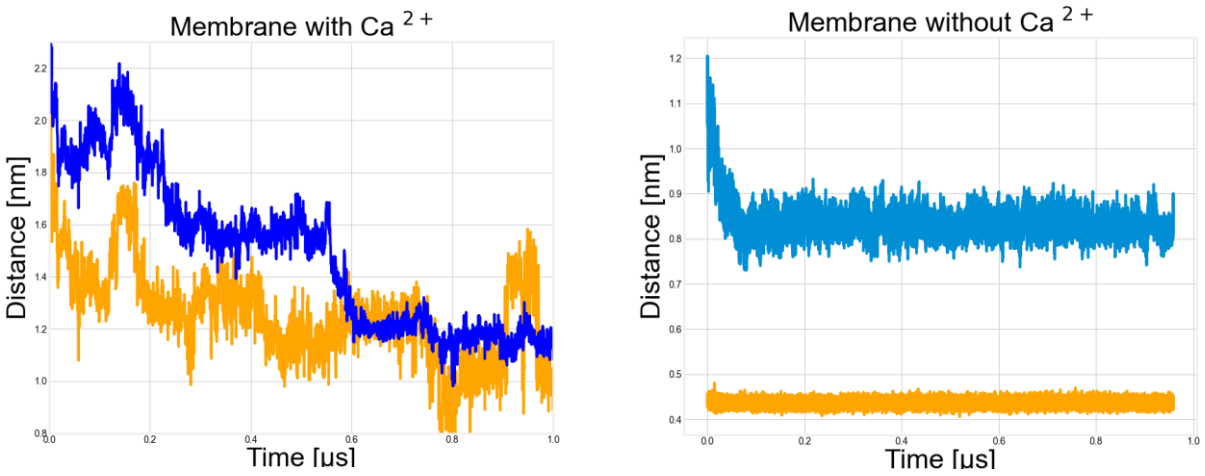

Fig. 3.6: Panel left: 1 µs of the unbiased simulation membrane with Ca^{2+}, blue: Average distance of AMPs sidechain to phosphate groups, orange: lysine sidechain distance to phosphate groups. Panel right: 1 µs of the unbiased simulation membrane without Ca^{2+}, blue: Average distance of AMPs sidechain to phosphate groups, orange: lysine sidechain distance to phosphate groups.

To determine if the interaction with positively charged amino acids increases, I also calculated the distance between the phosphate groups and lysine residues in Magainin 2. The distance between the sidechain of lysine (Fig. 3.6, orange) and phosphate groups in the membrane with Ca^{2+} ions are 1.2 nm. The distance between the sidechain of lysine and the phosphate groups in the membrane without Ca^{2+} ions is 0.45 nm. The smaller distance between the phosphate groups and the lysine in the simulation without Ca^{2+} ions indicates that the cationic sidechains of the AMP are coordinated directly to the phosphate groups when they do not have to compete with Ca^{2+} ions. This corresponds well with the hypothesis that the AMP must displace the Ca^{2+} ions to be able to have a strong interaction with the phosphate groups in the LPS layer.

3.3 Free energy profile

The unbiased simulation is not capable of sampling the entire energy surface. For this reason I perform umbrella sampling simulations to determine the free energy of insertion of the AMP into the bacterial envelope. The free energy profile is going allow us to detect the presence of energy barriers and where are the favorable interactions of the AMP and the membrane .

The free energy profile (Fig. 3.7) has a flat region with energy of roughly 0 kJ/mol in the interval +8 nm and +11 nm, which corresponds to the AMP being in bulk water. From +8 nm to +4 nm, the free energy decreases until reaching the global minimum of -300 kJ/mol at +4 nm, and the low energy indicates favourable interactions between the AMP and this section of the outer membrane. This section corresponds with the LPS layer in the bacterial outer membrane. From +4 nm to +2 nm, the free energy increases steadily to a maximum of 150 kJ/mol, corresponding to the beginning of the insertion process in the hydrophobic core. The free energy decreases again from 0 nm to -2 nm, reaching a local minimum of -100 kJ/mol at -2 nm. This minimum corresponds with the location of the phosphate groups in the inner layer. From -2 nm to -5 nm, the free energy increases again until it reaches a maximum of 100 kJ/mol. In this position, the peptide is near the water interface. From -6 nm to -11 nm, the free energy plateau near 0 kJ/mol corresponds to the bulk water.

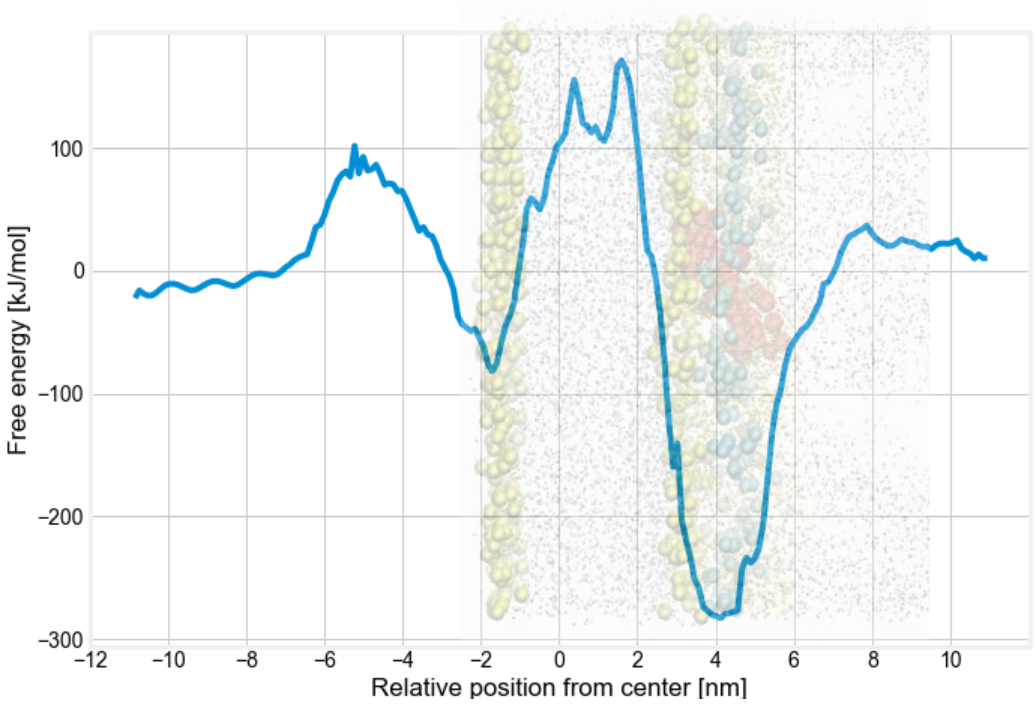

Fig.3.7: Free energy profile of Magainin 2 insertion across the Z coordinate in the outer bacterial membrane from +11 nm to -11 nm. The minimum of energy is found in at +4 nm inside the LPS layer. (In the back, a representation of the bacterial outer membrane: yellow phosphate groups of Lipid A, POPE, POPC, and CDL2, the light blue hydrophobic core of the membrane, dark blue the negatively charge groups in the LPS core, light red LPS).

The global minimum in the outer leaflet occurs when the protein center of mass is at 4 nm from the center of the membrane. At 4 nm, the peptide is in the LPS core. In this position in the cell envelope, the cationic peptide interacts with the Lipid A phosphate groups and the RALPS phosphate groups. This result indicates that the AMP forms an energetically favorable interaction with the LPS core before it inserts deeper into the membrane. This was only apparent in the free energy profile because the breadth of the minimum obscured this mode of interaction and the low frequency of spontaneous insertion events in the free MD simulations.

This result is in agreement with the theory presented by Freire *et al.*[41] that the LPS layer acts as an electrostatic barrier. Freire *et al.* also hypothesize that the capacity of the AMP to overcome this "sponge effect" is a matter of concentration. On another hand, the strong interaction with LPS layer can lead to more binding and the clustering of the AMP in the LPS layer. This interaction with the LPS layer is thought [80] to lead to a change in the secondary structure that can make possible the insertion in the membrane. Moreover, the antimicrobial activity and the insertion of the peptide in the membrane is modulated by the LPS/AMP interaction and because of this it is necessary to take the interaction into account for futures studies or design of the AMP for clinic use. These results indicate that in addition to optimizing AMP/lipid interactions, it is also important to consider AMP/LPS interactions.

At 0.5 nm and 1.7 nm, there are two maxima in the energy profile. This position corresponds with the hydrophobic core of Lipid A. Lyu *et al.* previously reported a free energy profile for the insertion of an AMP into a POPC bilayer with a maximum in the center of the bilayer [81]. In the Lyu *et al.* study, the free energy profile maximum is dependent on the number of AMPs in the interior of the membrane. They calculated the free energy profile of insertion of one AMP in a membrane with 0 to 6 peptides inserted. The aggregate of six peptides decreases the energy barrier to 0 [81]. The maxima I observe and the decrease of the maxima due to this oligomerization, observed by Lyu, can be due to the amphipathic nature of the Magainin 2, and the positive charges can affect the AMP stability in the membrane. This maximum and the effect of oligomerization are consistent with the proposal that Magainin 2 does not permeabilize the membrane by forming an organized toroidal pore but forms a disordered toroidal pore.

Chapter 4: Conclusion

In this thesis, molecular dynamic simulations were used for describing the interaction of the AMP Magainin 2 with the gram-negative bacterial outer membrane and, more specifically, the interaction with the LPS layer. As part of this effort, I constructed a coarse-grained Martini model of a realistic outer membrane form with an LPS outer layer with RALPS and O-ANT and a POPE, POPC, and cardiolipin inner layer. I then performed 25 μs of MD simulations of the membrane in the presence of the Magainin 2 AMP.

The membrane simulation reaches equilibrium after 15 μs of molecular dynamics simulation, and I used the equilibrated membrane to analyze the interaction between the membrane and the AMP. The composition of the model was analyzed using a density profile, and the positions of each peak were compared and generally agreed with previously reported membranes. Furthermore, the water profile drops to 0 for 2 nm around the center of the membrane, and this is consistent with a hydrophobic thickness of 2 nm.

In these unbiased MD simulations, I did not observe the insertion of the Magainin 2 peptide in the hydrophobic core of the bacterial membrane. Two previously presented hypotheses can explain why the AMP stays in the LPS layer during the simulation. One hypothesis is the "self-promoted-intake" of the AMP [39]; according to this, the AMP first interacts with the LPS phosphate groups ,displacing the Ca^{2+} ions that crosslink and stabilize the LPS layer. This distortion allows the insertion of the AMP in the membrane. The other hypothesis says that the LPS can act like an electrostatic barrier, "trapping" the AMP [41]. It is thus notable than when I calculated the distance between AMP and the membrane center, it shows that the peptide remained in the LPS section of the bacterial envelope throughout the entire simulation, and this supports the idea that the LPS layer can act by "trapping" the AMPs.

For analyzing if the AMP has an initial interaction with the AMP phosphate groups, I calculated the number of contacts between the phosphate groups and the AMP. The contact number through the simulation shows a minor interaction consistent with that reported for membranes crosslinked with Na^{+} [71]. Some differences are observed, likely because model membranes crosslinked with Ca^{2+} have a more rigid packing of the LPS layer. For further analysis, I compared two membranes when the LPS was crosslinked with Ca^{2+} and the other when the LPS

was not crosslinked with Ca^{2+}. For analyzing the impact of the Ca^{2+} in the interaction AMP-LPS, I calculated the minimal distance between the LPS phosphate groups and the AMP sidechain for the envelope with Ca^{2+} ions and without Ca^{2+} ions. The minimal distance was smaller in the membrane without Ca^{2+} suggesting a stronger interaction AMP-LPS.

The interaction AMP-LPS is an electrostatic interaction between the AMP charge groups and the LPS phosphate groups. For this reason, the calculation of the distance between Lysine and LPS phosphates groups can offer valuable information. The space from Lysine to LPS phosphates groups is smaller in the simulation without Ca^{2+}. The stronger AMP-LPS interaction in the simulation without Ca^{2+} ions correspond well with the hypothesis that the AMP must displace the strong interaction of the calcium with the phosphate groups in the LPS layer.

The presence of an electrostatic barrier in the LPS can be another reason for the peptide to remain in the LPS layer. To address this possibility, enhanced sampling techniques like umbrella sampling simulation are needed, because of the membrane's complexity and consequent challenges to exploring the whole energy surface. To calculate the free energy profile of insertion of the peptide, I performed an umbrella sampling simulation for 216 windows and calculated the free energy profile of the peptide in the membrane. The free energy profile shows a global minimum at +4 nm from the center of the membrane; this result agrees with the theory presented by Freire *et al.* [39] that the LPS layer acts as an electrostatic barrier and traps the AMP. The AMP “trapping" can increase the concentration of the AMP in the LPS layer and allow the insertion in the membrane. The free energy profile also shows a maximum in the center of the membrane. These maxima were previously reported [81]. It is consistent with the amphipathic nature of the Magainin 2 and the theory that Magainin 2 permeabilizes the membrane forming a disordered toroidal pore.

Chapter 5: Future Work

5.1 Convergence of Calculated Properties

The free energy profile has maxima at -5 nm in the water near to the interface (Fig 3.2). This behavior could be because free energy calculation is computationally expensive and challenging to converge when the membrane is formed with one layer of slow-moving LPS and another layer

of faster-moving phospholipids. LPS diffusion is an order of magnitude slower than that of phospholipids [74]. The slow diffusion rates of LPS resulted in a limited sampling of the configurational space. Different ways for achieving converged simulations have been proposed. These include elevating the temperature of the simulation with values over the physiological, substitute the divalent ions in the LPS layer for monovalent cations, and constructing the outer layer with a mix of phospholipids and LPS rather than just LPS [74].

The calculation of the free energy profile of Magainin 2 insertion into the bilayer required extensive simulations, and even then, it was not clear that the simulations converged. The large size of the AMP means the choice of center of mass difference between the AMP and the solute as the parameter to be varied is less appropriate than it is for simple solutes (e.g., small molecules). To calculate a free energy profile that provides a complete description of AMP insertion, it may be necessary to calculate the free energy profile in terms of multiple coordinates. The tilt angle of the peptide with respect to the plane of the membrane has been proposed to be a second important coordinate, so this would be an obvious secondary access to calculate the free energy profile.

5.2 Effects of AMP Dimerization

All the simulations performed here had one AMP in the simulation cell. There have been some proposals that Magainin 2 can form dimeric structures [82]. Simulations containing multiple AMPs in the simulation cell would be needed to describe this feature. The MARTINI model used in this research tends to overestimate the strength of protein-protein interactions, which would make them unsuitable for simulations of protein aggregation [78]. New MARTINI parameters have been developed to address this issue, so this type of simulation may be practical in the future [83].

5.3 Effects of the Coarse-Grain Model

The coarse-grain MARTINI model used in this thesis made it possible to simulate a membrane with reasonable spatial dimensions at a relatively long timescale. Nevertheless, the coarse nature of this model prevents us from examining atomic-scale interactions, like interactions between specific functional groups of the protein and the membrane. Ionic interactions are important in these systems, but specific ionic interactions are challenging for the MARTINI model. It may be necessary to model these systems using atomistic models.

Chapter 6- Appendix

6.1 MDP file for unbiased simulation

```
; VARIOUS PREPROCESSING OPTIONS
; Preprocessor information: use cpp syntax.

include                  =
; e.g.: -DPOSRES -DFLEXIBLE (note these variable names are case sensitive)
define                   = -DPOS_Z_AXES

; RUN CONTROL PARAMETERS
integrator               = md
; Start time and timestep in ps
tinit                    = 0.0
dt                       = 0.02
nsteps                   = 2000000000
; For exact run continuation or redoing part of a run
init-step                = 0
; Part index is updated automatically on checkpointing (keeps files separate)
simulation-part          = 1
; mode for center of mass motion removal
comm-mode                = Linear
; number of steps for center of mass motion removal
nstcomm                  = 1
; group(s) for center of mass motion removal
comm-grps                = membrane


; OUTPUT CONTROL OPTIONS
; Output frequency for coords (x), velocities (v) and forces (f)
nstxout                  = 9000000
nstvout                  = 9000000
nstfout                  = 0
; Output frequency for energies to log file and energy file'
nstlog                   = 25000
nstcalcenergy            = 100
nstenergy                = 25000
; Output frequency and precision for .xtc file
nstxtcout                = 25000
xtc_precision            = 100
; This selects the subset of atoms for the .xtc file. You can
; select multiple groups. By default all-atoms will be written.
xtc-grps                 =
; Selection of energy groups
energygrps               = protein membrane solute

; NEIGHBORSEARCHING PARAMETERS
```

```
; cut-off scheme (group: using charge groups, Verlet: particle based cut-
offs)
cutoff-scheme            = Group
; nblist update frequency
nstlist                  = 10
; ns algorithm (simple or grid)
ns_type                  = grid
; Periodic boundary conditions: xyz, no, xy
pbc                      = xyz
periodic-molecules       = no
; Allowed energy drift due to the Verlet buffer in kJ/mol/ps per atom,
; a value of -1 means: use rlist
verlet-buffer-drift      = 0.005
; nblist cut-off
rlist                    = 1.4
; long-range cut-off for switched potentials
rlistlong                = -1
nstcalclr                = -1

; OPTIONS FOR ELECTROSTATICS AND VDW
; Method for doing electrostatics
coulombtype              = Shift
rcoulomb_switch          = 0.0
rcoulomb                 = 1.2
; Relative dielectric constant for the medium and the reaction field
epsilon_r                = 15
epsilon_rf               = 1
; Method for doing Van der Waals
vdw_type                 = Shift
; cut-off lengths
rvdw_switch              = 0.9
rvdw                     = 1.2
; OPTIONS FOR WEAK COUPLING ALGORITHMS
; Temperature coupling
tcoupl                   = v-rescale
nsttcouple               = -1
nh-chain-length          = 10
print-nose-hoover-chain-variables = no
; Groups to couple separately
tc-grps                  = protein membrane solute
; Time constant (ps) and reference temperature (K)
tau_t                    = 1.0 1.0 1.0
ref_t                    = 310 310 310
; pressure coupling
Pcoupl                   = Parrinello-Rahman
Pcoupltype               = semiisotropic
nstpcouple               = -1
; Time constant (ps), compressibility (1/bar) and reference P (bar)
tau_p                    = 5.0
```

```
compressibility          = 3e-4 3e-4
ref_p                    = 1.0 1.0
; Scaling of reference coordinates, No, All or COM
refcoord_scaling         = all
gen_vel                  = no
continuation             = yes


; MARTINI and CONSTRAINTS
; for ring systems constraints are defined
; which are best handled using Lincs.
; Note, during energy minimization the constrainst should be
; replaced by stiff bonds.
constraints              = none
constraint_algorithm     = Lincs
lincs_order              = 4 ; can use order 6 iter 2
lincs_warnangle          = 90
```

6.2 Example of Input file for plumed Steered MD

```
#Reconstruct the protein and the membrane.
WHOLEMOLECULES STRIDE=1 ENTITY0=53-11704  ENTITY1=1-52

#COM of the membrane with PO and the peptide
p: GROUP NDX_FILE=index.ndx NDX_GROUP=PROTEIN
memb: GROUP NDX_FILE=index1.ndx NDX_GROUP=PO
com1: COM  ATOMS=memb
com2: COM  ATOMS=p

#Distance Peptide-membrane
dist: DISTANCE ATOMS=com1,com2 COMPONENTS NOPBC

# Add a lower and an upper wall on the peptide/membrane distance.
UPPER_WALLS ...
 ARG=dist.z
 AT=2.0
 KAPPA=1.0
 LABEL=uwall
... UPPER_WALLS

LOWER_WALLS ...
  ARG=dist.z
  AT=1.0
  KAPPA=1.0
  LABEL=lwall
... LOWER_WALLS
```

```
#Umbrella Sampling
MOVINGRESTRAINT ...
   ARG=dist.z
STEP0=0 AT0=11.0 KAPPA0=5000
STEP1=1000 AT1=10.9 KAPPA1=5000
STEP2=2000 AT2=10.8 KAPPA2=5000
STEP3=3000 AT3=10.7 KAPPA3=5000
STEP4=4000 AT4=10.6 KAPPA4=5000
STEP5=5000 AT5=10.5 KAPPA5=5000
STEP6=6000 AT6=10.4 KAPPA6=5000
STEP7=7000 AT7=10.3 KAPPA7=5000

... MOVINGRESTRAINT
PRINT STRIDE=10000 ARG=dist.z FILE=prueba.out
```

6.3 Input file for umbrella sampling simulation in Plumed-Gromacs:

```
#Reconstruct the protein and the membrane.
WHOLEMOLECULES STRIDE=1 ENTITY0=53-11704  ENTITY1=1-52

#COM of the membrane with PO and the peptide
p: GROUP NDX_FILE=index.ndx NDX_GROUP=PROTEIN
memb: GROUP NDX_FILE=index1.ndx NDX_GROUP=PO
com1: COM  ATOMS=memb
com2: COM  ATOMS=p
#Distance Peptide-membrane
dist: DISTANCE ATOMS=com1,com2 COMPONENTS NOPBC
# Impose an umbrella potential on com1 and com2
# with a spring constant of 00 kjoule/mol
#
restraint-com: RESTRAINT ARG=dist.z KAPPA=2000 AT=1.0
# monitor the two variables and the bias potential from the two
PRINT STRIDE=1000 ARG=dist.z,restraint-com.bias FILE=2000NEWALLCOVAR1.0
```

References

[1] Gould, “Antibiotics: from prehistory to the present day,” *J. Antimicrob. Chemother.*, vol. 71, no. 3, pp. 572–575, 2016, doi: 10.1093/JAC/DKV484.

[2] Kumar and Pal, “Antibiotic resistance and wastewater: Correlation, impact and critical human health challenges,” *J. Environ. Chem. Eng.*, vol. 6, pp. 52–58, 2017, doi: 10.1016/j.jece.2017.11.059.

[3] Egorov, Ulyashova, and Rubtsova, “Bacterial enzymes and antibiotic resistance,” *Acta Naturae*, vol. 10, no. 4. pp. 33–48, 2018. doi: 10.32607/20758251-2018-10-4-33-48.

[4] Minsky, Summers, and Knowles, “Secretion of β-lactamase into the periplasm of Escherichia coli: Evidence for a distinct release step associated with a conformational change,” *Proc. Natl. Acad. Sci. U. S. A.*, vol. 83, no. 12, pp. 4180–4184, 1986, doi: 10.1073/pnas.83.12.4180.

[5] Thakur, Uniyal, and Tiwari, “A comprehensive review on pharmacology of efflux pumps and their inhibitors in antibiotic resistance,” *Eur. J. Pharmacol.*, vol. 903, p. 174151, 2021, doi: 10.1016/j.ejphar.2021.174151.

[6] WHO, “Global action plan on antimicrobial resistance,” *World Heal. Organ.*, pp. 1–28, 2017.

[7] Lee and Aguilar, “Antimicrobial Peptide Structure and Mechanism of Action: A Focus on the Role of Membrane Structure,” *Current Topics in Medicinal Chemistry*, vol. 16, no. 1. pp. 25–39, 2016. doi: http://dx.doi.org/10.2174/1568026615666150703121700.

[8] Bahar and Ren, “Antimicrobial Peptides,” *Pharmaceuticals*, vol. 6, no. 12, p. 1543, 2013, doi: 10.3390/PH6121543.

[9] Zeya and Spitznagel, “Antibacterial and Enzymic Basic Proteins from Leukocyte Lysosomes: Separation and Identification,” *Science (80-.).*, vol. 142, no. 3595, pp. 1085–1087, 1963, doi: 10.1126/SCIENCE.142.3595.1085.

[10] Nakatsuji and Gallo, “Antimicrobial peptides: Old molecules with new ideas,” *Journal of Investigative Dermatology*, vol. 132, no. 3 P. pp. 887–895, 2012. doi: 10.1038/jid.2011.387.

[11] Steiner, Hultmark, Engström, Bennich, and Boman, “Sequence and specificity of two antibacterial proteins involved in insect immunity,” *Nature*, vol. 292, no. 5820, pp. 246–248, 1981, doi: 10.1038/292246a0.

[12] Zasloff, “Magainins, a class of antimicrobial peptides from Xenopus skin: Isolation, characterization of two active forms, and partial cDNA sequence of a precursor,” *Proc. Natl. Acad. Sci. U. S. A.*, vol. 84, no. 15, pp. 5449–5453, 1987, doi: 10.1073/pnas.84.15.5449.

[13] Hancock, “Cationic peptides: effectors in innate immunity and novel antimicrobials,” *Lancet Infect. Dis.*, vol. 1, no. 3, pp. 156–164, 2001, doi: 10.1016/S1473-3099(01)00092-5.

[14] Yeaman and Yount, “Mechanisms of Antimicrobial Peptide Action and Resistance,” *Pharmacol. Rev.*, vol. 55, no. 1, pp. 27–55, 2003, doi: 10.1124/pr.55.1.2.

[15] Magana, Pushpanathan, Santos, Leanse, Fernandez, Ioannidis, Giulianotti, Apidianakis, Bradfute, Ferguson, Cherkasov, Seleem, Pinilla, de la Fuente-Nunez, *et al.*, “The value of antimicrobial peptides in the age of resistance,” *The Lancet Infectious Diseases*, vol. 20, no. 9. pp. 216–230, 2020. doi: 10.1016/S1473-3099(20)30327-3.

[16] Pizzolato-Cezar, Okuda-Shinagawa, and Teresa Machini, “Combinatory therapy antimicrobial peptide-antibiotic to minimize the ongoing rise of resistance,” *Frontiers in Microbiology*, vol. 10. p. 1703, 2019. doi: 10.3389/fmicb.2019.01703.

[17] Datta and Roy, “Antimicrobial Peptides as Potential Therapeutic Agents: A Review,” *Int. J. Pept. Res. Ther.*, vol. 27, no. 1, pp. 555–577, 2021, doi: 10.1007/s10989-020-10110-x.

[18] Koehbach and Craik, “The Vast Structural Diversity of Antimicrobial Peptides,” *Trends in Pharmacological Sciences*, vol. 40, no. 7. pp. 517–528, 2019. doi: 10.1016/j.tips.2019.04.012.

[19] Aisenbrey, Marquette, and Bechinger, "The Mechanisms of Action of Cationic Antimicrobial Peptides Refined by Novel Concepts from Biophysical Investigations," in *Antimicrobial Peptides: Basics for Clinical Application*, Springer Singapore, 2019, pp. 33–64. doi: 10.1007/978-981-13-3588-4_4.

[20] Sengupta, Leontiadou, Mark, and Marrink, "Toroidal pores formed by antimicrobial peptides show significant disorder," *Biochim. Biophys. Acta*, vol. 1778, pp. 2308–2317, 2008, doi: 10.1016/j.bbamem.2008.06.007.

[21] Zerweck, Strandberg, Kukharenko, Reichert, Bürck, Wadhwani, and Ulrich, "Molecular mechanism of synergy between the antimicrobial peptides PGLa and magainin 2," *Sci. Rep.*, vol. 7, no. 1, 2017, doi: 10.1038/s41598-017-12599-7.

[22] Gesell, Zasloff, and Opella, "Two-dimensional 1 H NMR experiments show that the 23-residue magainin antibiotic peptide is an α α-helix in dodecylphosphocholine micelles, sodium dodecylsulfate micelles, and trifluoroethanol/water solution," *J. Biomol. NMR*, vol. 9, pp. 127–135, 1997.

[23] Berman, Westbrook, Feng, Gilliland, Bhat, Weissig, Sgindyalov, and Bourne, "The Protein Data Bank," *Nucleic Acids Res.*, vol. 28, pp. 235–242, 2000, doi: doi:10.1093/nar/28.1.235.

[24] Matsuzaki, Sugishita, Harada, Fujii, and Miyajima, "Interactions of an antimicrobial peptide, magainin 2, with outer and inner membranes of Gram-negative bacteria," *Biochim. Biophys. Acta*, vol. 1327, no. 1, pp. 119–130, 1997, doi: 10.1016/S0005-2736(97)00051-5.

[25] Thwaite, Humphrey, Fox, Savage, Laws, Ulaeto, Titball, and Atkins, "The cationic peptide magainin II is antimicrobial for Burkholderia cepacia-complex strains," *J. Med. Microbiol.*, vol. 58, no. 7, pp. 923–929, 2009, doi: 10.1099/JMM.0.008128-0.

[26] Hallock, Lee, and Ramamoorthy, "MSI-78 , an Analogue of the Magainin Antimicrobial Peptides , Disrupts Lipid Bilayer Structure via Positive Curvature Strain," *Biophys. J.*, vol. 84, no. 5, pp. 3052–3060, 2003, doi: 10.1016/S0006-3495(03)70031-9.

[27] Khatami, Bromberek, Saika-Voivod, and Booth, "Molecular dynamics simulations of histidine-containing cod antimicrobial peptide paralogs in self-assembled bilayers,"

Biochim. Biophys. Acta - Biomembr., vol. 1838, no. 11, pp. 2778–2787, 2014, doi: 10.1016/j.bbamem.2014.07.013.

[28] Field, Qi, Ingo, Cheng, Lee, Marrink, Im, Ingólfsson, Cheng, Lee, Marrink, and Im, "CHARMM-GUI Martini Maker for Coarse-Grained Simulations with the Martini Force Field," *J. Chem. Theory Comput.*, vol. 11, no. 9, pp. 4486–4494, 2015, doi: 10.1021/acs.jctc.5b00513.

[29] Chen, Starr, Troendle, Wiedman, Wimley, Ulmschneider, and Ulmschneider, "Simulation-Guided Rational de Novo Design of a Small Pore-Forming Antimicrobial Peptide," *J. Am. Chem. Soc.*, vol. 141, no. 12, pp. 4839–4848, 2019, doi: 10.1021/jacs.8b11939.

[30] Kabanov and Prokhorenko, "Structural analysis of lipopolysaccharides from gram-negative bacteria," *Biochem.*, vol. 75, no. 4, pp. 383–404, 2010, doi: 10.1134/S0006297910040012.

[31] Raetz and Whitfield, "Lipopolysaccharide Endotoxins," *Annu. Rev. Biochem*, vol. 71, pp. 635–700, 2003, doi: 10.1146/ANNUREV.BIOCHEM.71.110601.135414.

[32] Duerr, Zenk, Chassin, Pott, and Gü Tle, "O-Antigen Delays Lipopolysaccharide Recognition and Impairs Antibacterial Host Defense in Murine Intestinal Epithelial Cells," *PLoS Pathog*, vol. 5, no. 9, p. 1000567, 2009, doi: 10.1371/journal.ppat.1000567.

[33] Wimley and Hristova, "Antimicrobial Peptides: Successes, Challenges and Unanswered Questions," *J. Membr. Biol.*, vol. 239, no. 1, pp. 27–34, Jan. 2011, doi: 10.1007/s00232-011-9343-0.

[34] Song, de Groot, and Sansom, "Lipid Bilayer Composition Influences the Activity of the Antimicrobial Peptide Dermcidin Channel," *Biophys. J.*, vol. 116, no. 9, pp. 1658–1666, 2019, doi: 10.1016/j.bpj.2019.03.033.

[35] Leontiadou, Mark, and Marrink, "Antimicrobial Peptides in Action clawed frog Xenopus lae V is 1 that exhibit a wide range of," no. 9, pp. 12156–12161, 2006, doi: 10.1021/ja062927q.

[36] Wimley, "Describing the mechanism of Antimicrobial Peptide action with the interfacial

Activity model," *ACS Chem. Biol.*, vol. 5, no. 10, pp. 905–917, 2010, doi: 10.1021/cb1001558.

[37] Ebbensgaard, Mordhorst, Aarestrup, and Hansen, "The Role of Outer Membrane Proteins and Lipopolysaccharides for the Sensitivity of Escherichia coli to Antimicrobial Peptides," *Front. Chem.*, vol. 9, no. 2153, pp. 1–13, 2018, doi: 10.3389/fmicb.2018.02153.

[38] Schmidtchen and Malmsten, "Peptide interactions with bacterial lipopolysaccharides," *Curr. Opin. Colloid Interface Sci.*, vol. 18, no. 5, pp. 381–392, 2013, doi: 10.1016/j.cocis.2013.06.003.

[39] Hancock and Rozek, "Role of membranes in the activities of antimicrobial cationic peptides," *FEMS Microbiol. Lett.*, vol. 206, no. 2, pp. 143–149, 2002, doi: 10.1016/S0378-1097(01)00480-3.

[40] Malanovic and Lohner, "Gram-positive bacterial cell envelopes: The impact on the activity of antimicrobial peptides," *Biochim. Biophys. Acta - Biomembr.*, vol. 1858, no. 5, pp. 936–946, 2016, doi: 10.1016/J.BBAMEM.2015.11.004.

[41] Freire, Gaspar, Veiga, and Castanho, "Shifting gear in antimicrobial and anticancer peptides biophysical studies: from vesicles to cells," *J. Pept. Sci.*, vol. 21, no. 3, pp. 178–185, 2015, doi: 10.1002/PSC.2741.

[42] Marrink, Corradi, Souza, Ingólfsson, Tieleman, and Sansom, "Computational Modeling of Realistic Cell Membranes," *Chemical Reviews*, vol. 119, no. 9. pp. 6184–6226, 2019. doi: 10.1021/acs.chemrev.8b00460.

[43] Karplus and McCammon, "Molecular dynamics simulations of biomolecules," *Nat. Struct. Biol.*, vol. 9, no. 9, pp. 646–652, 2002, doi: 10.1038/nsb0902-646.

[44] Klauda, Venable, Freites, Connor, Tobias, Mondragon-ramirez, Vorobyov, Mackerell, and Pastor, "Update of the CHARMM All-Atom Additive Force Field for Lipids : Validation on Six Lipid Types," *J. Phys. Chem.*, vol. 2, pp. 7830–7843, 2010, doi: 10.1021/jp101759q.

[45] Best, Zhu, Shim, Lopes, Mittal, Feig, and Alexander D. MacKerell, "Optimization of the

Additive CHARMM All-Atom Protein Force Field Targeting Improved Sampling of the Backbone ϕ, ψ and Side-Chain χ1 and χ2 Dihedral Angles," *J. Chem. Theory Comput.*, vol. 8, no. 9, pp. 3257–3273, 2012, doi: 10.1021/CT300400X.

[46] Dickson, Madej, Skjevik, Betz, Teigen, Gould, and Walker, "Lipid14: The amber lipid force field," *J. Chem. Theory Comput.*, vol. 10, no. 2, pp. 865–879, 2014, doi: 10.1021/ct4010307.

[47] Wang, Wolf, Caldwell, Kollman, and Case, "Development and testing of a general amber force field," *J. Comput. Chem.*, vol. 25, no. 9, pp. 1157–1174, 2004, doi: 10.1002/JCC.20035.

[48] Grote and Lyubartsev, "Optimization of Slipids Force Field Parameters Describing Headgroups of Phospholipids," *J. Phys. Chem. B*, vol. 124, no. 40, pp. 8784–8793, 2020, doi: 10.1021/acs.jpcb.0c06386.

[49] Reif, Winger, and Oostenbrink, "Testing of the GROMOS force-field parameter set 54A8: Structural properties of electrolyte solutions, lipid bilayers, and proteins," *J. Chem. Theory Comput.*, vol. 9, no. 2, pp. 1247–1264, 2013, doi: 10.1021/ct300874c.

[50] Saunders and Voth, "Coarse-Graining Methods for Computational Biology," *Annu. Rev. Biophys.*, vol. 42, no. 1, pp. 73–93, 2013, doi: 10.1146/annurev-biophys-083012-130348.

[51] Marrink and Tieleman, "Perspective on the Martini model.," *Chem. Soc. Rev.*, vol. 42, no. 16, pp. 6801–6822, 2013, doi: 10.1039/c3cs60093a.

[52] Allen and Rutledge, "A novel algorithm for creating coarse-grained, density dependent implicit solvent models," *J. Chem. Phys.*, vol. 128, no. 15, p. 154115, 2008, doi: 10.1063/1.2899729.

[53] Joshi and Deshmukh, "A review of advancements in coarse-grained molecular dynamics simulations," *Mol. Simul.*, pp. 1–18, 2020, doi: 10.1080/08927022.2020.1828583.

[54] Marrink, Risselada, Yefimov, Tieleman, and De Vries, "The MARTINI force field: Coarse grained model for biomolecular simulations," *J. Phys. Chem. B*, vol. 111, no. 27, pp. 7812–7824, 2007, doi: 10.1021/jp071097f.

[55] Im and Khalid, “Molecular Simulations of Gram-Negative Bacterial Membranes Come of Age,” *Annu. Rev. Phys. Chem.*, vol. 71, no. 1, pp. 171–188, 2020, doi: 10.1146/annurev-physchem-103019-033434.

[56] Shearer, Jefferies, and Khalid, “Outer Membrane Proteins OmpA, FhuA, OmpF, EstA, BtuB, and OmpX Have Unique Lipopolysaccharide Fingerprints,” *J. Chem. Theory Comput.*, vol. 15, no. 4, pp. 2608–2619, 2019, doi: 10.1021/acs.jctc.8b01059.

[57] Shearer and Khalid, “Role of O - Antigen in Response to Mechanical Stress of the E. coli Outer Membrane: Insights from Coarse-Grained MD Simulations,” *J. Chem. Phys.*, vol. 123, pp. 3567–3575, 2019, doi: 10.1021/acs.jpcb.8b12168.

[58] Hsu, Bruininks, Jefferies, Cesar Telles de Souza, Lee, Patel, Marrink, Qi, Khalid, Im, Souza, Lee, Patel, Marrink, *et al.*, “Charmm-gui martini maker for modeling and simulation of complex bacterial membranes with lipopolysaccharides,” *J. Comput. Chem.*, vol. 38, no. 27, pp. 2354–2363, Oct. 2017, doi: 10.1002/jcc.24895.

[59] Kirschner, Lins, Maass, and Soares, “A glycam-based force field for simulations of lipopolysaccharide membranes: Parametrization and validation,” *J. Chem. Theory Comput.*, vol. 8, no. 11, pp. 4719–4731, 2012, doi: 10.1021/ct300534j.

[60] Hwang, Paracini, Parks, Lakey, and Gumbart, “Distribution of mechanical stress in the Escherichia coli cell envelope,” *Biochim. Biophys. Acta - Biomembr.*, vol. 1860, no. 12, pp. 2566–2575, 2018, doi: 10.1016/j.bbamem.2018.09.020.

[61] Bond, Holyoake, Ivetac, Khalid, and Sansom, “Coarse-grained molecular dynamics simulations of membrane proteins and peptides,” *J. Struct. Biol.*, vol. 157, no. 3, pp. 593–605, 2007, doi: 10.1016/j.jsb.2006.10.004.

[62] Berendsen, Postma, Gunsteren, DiNola, and Haak, “Molecular dynamics with coupling to an external bath,” *J. Chem. Phys.*, vol. 81, no. 8, p. 3684, 1998, doi: 10.1063/1.448118.

[63] Bussi, Donadio, and Parrinello, “Canonical sampling through velocity rescaling,” *J. Chem. Phys.*, vol. 126, no. 1, p. 014101, 2007, doi: 10.1063/1.2408420.

[64] Hoover, “Canonical dynamics: Equilibrium phase-space distributions,” *Phys. Rev. A*, vol. 31, no. 3, p. 1695, 1985, doi: 10.1103/PhysRevA.31.1695.

[65] Kästner, “Umbrella sampling,” *Wiley Interdiscip. Rev. Comput. Mol. Sci.*, vol. 1, no. 6, pp. 932–942, 2011, doi: 10.1002/WCMS.66.

[66] Hub, De Groot, and Van Der Spoel, “G-whams-a free Weighted Histogram Analysis implementation including robust error and autocorrelation estimates,” *J. Chem. Theory Comput.*, vol. 6, no. 12, pp. 3713–3720, 2010, doi: 10.1021/ct100494z.

[67] Spoel, Lindahl, Hess, Groenhof, Mark, and Berendsen, “GROMACS: Fast, flexible, and free,” *J. Comput. Chem.*, vol. 26, no. 16, pp. 1701–1718, 2005, doi: 10.1002/JCC.20291.

[68] Jo, Kim, Iyer, and Im, “CHARMM-GUI: A web-based graphical user interface for CHARMM,” *J. Comput. Chem.*, vol. 29, no. 11, pp. 1859–1865, 2008, doi: 10.1002/JCC.20945.

[69] Wu, Cheng, Jo, Rui, Song, Dávila-Contreras, Qi, Lee, Monje-Galvan, Venable, Klauda, and Im, “CHARMM-GUI Membrane Builder toward realistic biological membrane simulations,” *J Comput Chem*, vol. 35, no. 27, pp. 1997–2004, 2014, doi: 10.1002/JCC.23702.

[70] Piggot, Holdbrook, and Khalid, “Electroporation of the E. coli and S. aureus membranes: Molecular dynamics simulations of complex bacterial membranes,” *J. Phys. Chem. B*, vol. 115, no. 45, pp. 13381–13388, 2011, doi: 10.1021/jp207013v.

[71] Hsu and Khalid, “Through the Lipopolysaccharide Glass: A Potent Antimicrobial Peptide Induces Phase Changes in Membranes,” *Biochemistry*, vol. 56, pp. 1672–1679, 2017, doi: 10.1021/acs.biochem.6b01063.

[72] Tribello, Bonomi, Branduardi, Camilloni, and Bussi, “PLUMED 2: New feathers for an old bird,” *Comput. Phys. Commun.*, vol. 185, no. 2, pp. 604–613, 2013, doi: 10.1016/j.cpc.2013.09.018.

[73] Alan Grossfiled, “WHAM: the weighted histogram analysis method.” [Online]. Available:

http://membrane.urmc.rochester.edu/wordpress/?page_id=126

[74] Shearer, Marzinek, Bond, and Khalid, "Molecular Dynamics Simulations of Bacterial Outer 1 Membrane Lipid Extraction: Adequate Sampling?," *bioRxiv*, 2020, doi: 10.1101/2020.06.11.146001.

[75] Nguyen, Gumbart, and Jensen, "Coarse-grained molecular dynamics simulations of the bacterial cell wall," in *Methods in Molecular Biology*, vol. 1440, 2016, pp. 247–270. doi: 10.1007/978-1-4939-3676-2_18.

[76] Hughes, Patel, Widmalm, Klauda, Clifton, Im, Hughes, and Patel, "Physical Properties of Bacterial Outer Membrane Models: Neutron Reflectometry & Molecular Simulation," *Biophys. J.*, vol. 116, no. 6, pp. 1095–1104, 2019, doi: 10.1016/j.bpj.2019.02.001.

[77] Irudayanathan, Jiang, and Nangia, "Simulating Gram-Negative Bacterial Outer Membrane: A Coarse Grain Model," *J. Phys. Chem. B*, vol. 119, no. 46, pp. 14668–14682, 2015, doi: 10.1021/acs.jpcb.5b07122.

[78] Gao, Lee, Widmalm, and Im, "Modeling and Simulation of Bacterial Outer Membranes with Lipopolysaccharides and Enterobacterial Common Antigen," *J. Phys. Chem. B*, vol. 124, no. 28, pp. 5948–5956, 2020, doi: 10.1021/acs.jpcb.0c03353.

[79] Ma, Cummins, Edelstein, Gomez, Khan, Llewellyn, Picudella, Willsey, and Nangia, "Modeling Diversity in Structures of Bacterial Outer Membrane Lipids," *J. Chem. Theory Comput.*, vol. 13, no. 2, pp. 811–824, 2017, doi: 10.1021/acs.jctc.6b00856.

[80] Freire, Gaspar, De La Torre, Veiga, Andreu, and Castanho, "Monitoring antibacterial permeabilization in real time using time-resolved flow cytometry," *Biochim. Biophys. Acta - Biomembr.*, vol. 1848, no. 2, pp. 554–560, 2015, doi: 10.1016/J.BBAMEM.2014.11.001.

[81] Lyu, Xiang, Zhu, and Narsimhan, "Potential of mean force for insertion of antimicrobial peptide melittin into a pore in mixed DOPC/DOPG lipid bilayer by molecular dynamics simulation," *J. Chem. Phys.*, vol. 146, no. 15, 2017, doi: 10.1063/1.4979613.

[82] Porcelli, Buck-koehntop, Thennarasu, Ramamoorthy, and Veglia, "Structures of the

Dimeric and Monomeric Variants of Magainin Antimicrobial Peptides (MSI-78 and MSI-594) in Micelles and Bilayers , Determined by NMR," *Biochemistry*, vol. 45, pp. 5793–5799, 2006, doi: 10.1021/bi0601813.

[83] Souza, Alessandri, Barnoud, Thallmair, Faustino, Grünewald, Patmanidis, Abdizadeh, Bruininks, Wassenaar, Kroon, Melcr, Nieto, Corradi, *et al.*, "Martini 3: a general purpose force field for coarse-grained molecular dynamics," *Nat. Methods 2021 184*, vol. 18, no. 4, pp. 382–388, 2021, doi: 10.1038/s41592-021-01098-3.